Microglial-glucocorticoid receptor depletion alters the response of hippocampal microglia and neurons in a chronic unpredictable mild stress paradigm in female mice

Picard, Katherine ; Bisht, Kanchan ; Poggini, Silvia ; Garofalo, Stefano ; Golia, Maria Teresa ; Basilico, Bernadette ; Abdallah, Fatima ; Ciano Albanese, Naomi ; Amrein, Irmgard ; Vernoux, Nathalie ; Sharma, Kaushik ; Hui, Chin Wai ; Savage, Julie C ; Limatola, Cristina ; Ragozzino, Davide ; Maggi, Laura ; Branchi, Igor ; Tremblay, Marie-Ève

DOI: https://doi.org/10.1016/j.bbi.2021.07.022

Microglial-glucocorticoid receptor depletion alters the response of hippocampal microglia and neurons in a chronic unpredictable mild stress paradigm in female mice

Katherine Picard*[1,2,3], Kanchan Bisht*[1], Silvia Poggini*[4], Stefano Garofalo[5], Maria Teresa Golia[5], Bernadette Basilico[5,6], Fatima Abdallah[4], Naomi Ciano Albanese[4,6], Irmgard Amrein[7], Nathalie Vernoux[1], Kaushik Sharma[1], Chin Wai Hui[1], Julie C. Savage[1], Cristina Limatola[5,8], Davide Ragozzino[#5], Laura Maggi[#5], Igor Branchi[#4], and Marie-Ève Tremblay[#1,2,3,9]

[1]Axe neurosciences, Centre de recherche du CHU de Québec–Université Laval, Québec, QC, Canada.

[2]Molecular Medicine Department, Université Laval, Québec City, QC, Canada.

[3]Division of Medical Sciences, University of Victoria, Victoria, BC, Canada.

[4]Center for Behavioral Sciences and Mental Health, Istituto Superiore di Sanità, Rome, Italy.

[5]Department of Physiology and Pharmacology, Istituto Pasteur-Fondazione Cenci Bolognetti, Sapienza University of Rome, Italy.

[6]Institute of Science and Technology (IST) Austria, Klosterneuburg, Austria.

[7]Functional Neuroanatomy, Institute of Anatomy, University of Zürich, Zurich, Switzerland.

[8]IRCCS Neuromed, Pozzilli, Italy.

[9]The Department of Biochemistry and Molecular Biology, The University of British Columbia, Vancouver, BC, Canada.

*Equal contribution as first authors
[#]Equal contribution as senior authors

Corresponding Author:
Dr. Marie-Ève Tremblay
Division of Medical Sciences
University of Victoria
Medical Sciences building, room 322
Victoria, BC V8P 5C2 Canada
evetremblay@uvic.ca

Conflict of interest statement

The authors declare no competing financial interests.

Data sharing statement

The data that support the findings of this study are available from the corresponding authors upon reasonable request.

Word count

10072 without abstract, 10445 with abstract

Abstract

Chronic psychological stress is one of the most important triggers and environmental risk factors for neuropsychiatric disorders. Chronic stress can influence all organs via the secretion of stress hormones, including glucocorticoids by the adrenal glands, which coordinate the stress response across the body. In the brain, glucocorticoid receptors (GR) are expressed by various cell types including microglia, which are its resident immune cells regulating stress-induced inflammatory processes. To study the roles of microglial GR under normal homeostatic conditions and following chronic stress, we generated a mouse model in which the GR gene is depleted in microglia specifically at adulthood to prevent developmental confounds. We first confirmed that microglia were depleted in GR in our model in males and females among the cingulate cortex and the hippocampus, both stress-sensitive brain regions. Then, cohorts of microglial-GR depleted and wild-type (WT) adult female mice were housed for 3 weeks in a standard or stressful condition, using a chronic unpredictable mild stress (CUMS) paradigm. CUMS induced stress-related behavior in both microglial-GR depleted and WT animals as demonstrated by a decrease of both saccharine preference and progressive ratio breakpoint. Nevertheless, the hippocampal microglial and neural mechanisms underlying the adaptation to stress occurred differently between the two genotypes. Upon CUMS exposure, microglial morphology was altered in the WT controls, without any apparent effect in microglial-GR depleted mice. Furthermore, in the standard environment condition, GR depleted-microglia showed increased expression of pro-inflammatory genes, and genes involved in microglial homeostatic functions (such as *Trem2*, *Cx3cr1* and *Mertk*). On the contrary, in CUMS condition, GR depleted-microglia showed reduced expression levels of pro-inflammatory genes and increased neuroprotective as well as anti-inflammatory genes compared to WT-microglia. Moreover, in microglial-GR depleted mice, but not in WT mice, CUMS led to a

significant reduction of CA1 long-term potentiation and paired-pulse ratio. Lastly, differences in adult hippocampal neurogenesis were observed between the genotypes during normal homeostatic conditions, with microglial-GR deficiency increasing the formation of newborn neurons in the dentate gyrus subgranular zone independently from stress exposure. Together, these findings indicate that, although the deletion of microglial GR did not prevent the animal's ability to respond to stress, it contributed to modulating hippocampal functions in both standard and stressful conditions, notably by shaping the microglial response to chronic stress.

Keywords

Microglia, glucocorticoid receptor, depletion, mouse model, chronic unpredictable mild stress, synaptic plasticity, behavior, neurogenesis, depression

Highlights

1) Microglial morphology is altered following stress in control but not mGR dep mice
2) mGR dep modulates microglial gene expression at steady-state and under stress
3) Hippocampal synaptic plasticity is altered by stress exposure only in mGR dep mice
4) Hippocampal neurogenesis is increased in mGR dep mice, independently from stress

1 Introduction

Stress is defined as the perturbation of the physiological homeostasis or psychological well-being by a real or interpreted threat. While the stress response is a necessary survival mechanism required for the adaptation to environmental challenges, it can have many adverse effects when it persists or is repeated over time (McEwen, 2008). Chronic stress is associated with an increased risk of developing adverse health conditions that include cardiovascular diseases (Steptoe and Kivimäki, 2012), neuropsychiatric disorders (Davis et al., 2017) and neurodegenerative diseases (Esch et al., 2002). In our modern society thriving on performance and efficiency, chronic stress is an increasingly important public health concern.

Stress activates the hypothalamic-pituitary-adrenal axis (HPA axis), which controls the production of glucocorticoids (GCs) by the adrenal cortex (Herman et al., 2016). GCs are a class of steroid hormones that regulate the physiological (e.g., metabolic, cardiovascular, and immune) and behavioral (e.g., emotional, cognitive, and motor) response to stress (Smith and Vale, 2006). The main GC in rodents is corticosterone (CORT), which acts by binding to mineralocorticoid receptors (MR) and GC receptors (GR). MR and GR cooperatively regulate the stress response (de Kloet et al., 2008; Orchinik et al., 1991). Nevertheless, MR is mainly recruited under basal conditions and GR upon stress, since MR has a 10-fold higher affinity for CORT (Reul and de Kloet, 1985). CORT has an anti-inflammatory effect that depends on its concentration and duration of exposure. Chronically elevated CORT levels, as measured upon chronic stress, repress mRNA levels of the neuronal chemokine fractalkine and its microglial CX3C chemokine receptor 1 (CX3CR1) –a signaling pathway that restrains neuroinflammation and modulates the stress response– while increasing mRNA levels of the pro-inflammatory cytokine interleukin (IL)-1β in

adult rat hippocampus (Sorrells et al., 2014). Long-term increase of CORT levels is also well-known to cause maladaptive neuronal plasticity, notably in the hippocampus. It has been shown that chronically elevated circulating CORT levels induce hippocampal dendritic retractions in ovariectomized females rats (McLaughlin et al., 2005) as well as neuronal loss and dendritic atrophy, leading to an overall reduction of hippocampal volume in male rodents (Lee et al., 2009; Sapolsky et al., 1985; Woolley et al., 1990). In female and male mice, chronic stress was also associated with a reduction of adult neurogenesis in the dentate gyrus (DG), the main region where new neurons are generated throughout life (Goshen et al., 2008; Murray et al., 2008).

Microglia, the resident macrophages of the brain, play an essential role in the maintenance and remodeling of neuronal networks. These cells modulate hippocampal neurogenesis by producing pro-neurogenic factors and phagocytosing the excess of newborn cells undergoing apoptosis (Sierra et al., 2014). Their processes are highly dynamic and make frequent contacts with neuronal cells at synapses (Tremblay et al., 2010). Microglia-synapse interactions were shown to be important for the formation, maintenance and elimination of synapses, contributing to processes such as synaptic plasticity, learning, and adaptation to the environment (Tay et al., 2017). Microglia are extremely sensitive to homeostatic changes in their microenvironment such as those resulting from chronic stress exposure. Several studies have revealed that microglia undergo important morphological and functional changes in response to chronic psychological stress (reviewed in (Picard et al., 2021)). In mice, different models of chronic stress were shown to exacerbate microglial phagocytosis, notably of synaptic structures (Lehmann et al., 2016; Milior et al., 2016; Wohleb et al., 2018). Stressed microglia also contribute to neuroinflammation via their secretion of various mediators. Indeed, in a paradigm of repeated social defeat, acutely isolated microglia from male mice had increased mRNA levels of IL-1β (Wohleb et al., 2011).

These modifications in response to chronic stress suggest microglial involvement in stress-induced neuronal deficits and behavioral maladaptation. However, while microglia abundantly express GR as demonstrated in rodent models (Sierra et al., 2008; Tanaka et al., 1997), the role of microglial GR under homeostatic conditions and in the stress response remains largely undetermined.

To explore the role of microglial GR in the response to stress, we generated a mouse model in which microglia specifically lack GR. We hypothesized that disrupting microglial GR signaling will modify their homeostatic functions, with consequences on the neurobehavioral response to stress. We crossed GRflox mice with Cx3cr1CreERT2 mice, resulting in a tamoxifen-inducible conditional depletion of GR from CX3CR1-expressing cells. Mice were treated with tamoxifen at adulthood to prevent developmental confounds, and the experiments were initiated one month after recombination, to target microglia selectively considering the higher turnover rate of peripheral myeloid cells that can also express CX3CR1 and transit to the brain upon stress (Lawson et al., 1992; Wohleb et al., 2013). Females were specifically examined considering their greater stress vulnerability and HPA axis dysregulation, as well as higher predisposition to stress-induced anxiety and depression compared with males (Heck and Handa, 2019). Female mice exposed to chronic unpredictable stress also presented increased glucocorticoid resistance compared to males, which might contribute to their vulnerability to stress-related disorders (Palumbo et al., 2020). The microglial-GR (mGR) depleted female mice and their wild-type (WT) controls were exposed either to standard housing conditions or chronic unpredictable mild stress (CUMS) using the Intellicage system, a high throughput apparatus designed for the automated behavioral phenotyping of mice (Kiryk et al., 2020). Our analyses focused on the hippocampus considering its high expression levels of GR and its key involvement in the stress response (de Kloet et al., 2005). We investigated microglial density, distribution and morphology, as well as gene

expression. We also assessed hippocampal neurogenesis, short- and long-term neuronal plasticity as well as basal synaptic transmission at Schaffer collateral-Cornu Ammonis 1 (CA1) synapses and in pyramidal neurons to provide insights into neural plasticity mechanisms underlying the response to CUMS (Tay et al., 2017).

2 Methods

2.1 Animals

All experiments were approved and performed under the guidelines of Université Laval's animal ethics committees, the Canadian Council on Animal Care, the European Directive (2010/63/UE), and the Italian legislation on animal experimentation (Decreto Legislativo 26/2014). Animals were examined for signs of discomfort as indicated by the animal care and use guidelines [National Academy of Sciences. Guide for the care and use of laboratory animals, 1998, ‘‘Guidelines for the Care and Use of Mammals in Neuroscience and Behavioral Research” (National Research Council 2003)]. They were housed at 22–25°C under a 12-h light-dark cycle with *ad libitum* access to food and water. The Cx3cr1CreERT2 mice were obtained from the European Mouse Mutant Archive with authorization from Prof. Steffen Jung (Weizmann Institute of Science, Rehovot, Israël) and crossed with Nr3c1 fl/fl (GRflox) mice purchased from The Jackson Laboratory (strain No. 021021). To induce recombination in Cx3cr1CreERT2+/-:Nr3c1fl/fl mice, at adulthood (6.5 to 8.5 weeks of age), the animals were treated orally with 10mg of tamoxifen (Sigma-Aldrich) (dissolved in 1:10 ethanol/corn oil) (microglial-GR depletion tamoxifen group) twice with a 2-day interval. As controls, Cx3cr1CreERT2+/-:Nr3c1fl/fl mice were treated with oil (microglial-GR depletion oil group), Cx3cr1CreERT2-/-:Nr3c1fl/fl mice with tamoxifen (WT tamoxifen group), and

Cx3cr1CreERT2-/-:Nr3c1fl/fl mice with oil (WT oil group). The animals were then allowed a resting period of 7-9 weeks, housed 3-5 per cage. This resting period allowed to selectively target microglia due to their longer lifespan compared with peripheral myeloid cells that can also express CX3CR1 (Füger et al., 2017). As described below, the animals were then either sacrificed to characterize microglial-GR depletion or transferred to the Intellicage system to study the effects of CUMS *versus* standard housing conditions, followed by behavioral, electrophysiological, cellular, or molecular analyses.

The physiological and behavioral features of the stress response profoundly differ between sexes (Figueiredo et al., 2002; Oyola and Handa, 2017). Numerous recent findings show that gonadal hormones might play a role in determining microglial response to stress, which could shape neurobiological and behavioral outcomes (Picard et al., 2021). Females have been reported to be more vulnerable to chronic stress and display an increased predisposition to stress-induced anxiety and depression (Heck and Handa, 2019). Therefore, considering both the higher vulnerability and the limited knowledge available from the literature, we decided in the current study to investigate the effects of microglial-GR deficiency in female subjects.

2.2 Characterization of microglial GR depletion

We first characterize microglial GR depletion in both males and females to confirm our model using immunofluorescence (Fourgeaud et al., 2016; Zhou et al., 2020). Naïve male and female mice were anesthetized with a mix of ketamine [80mg/kg]/xylazine [10mg/kg] and blood was transcardially flushed with ice-cold phosphate-buffered saline [50mM, pH 7.40] (PBS). Brains were post-fixed in 4% paraformaldehyde (PFA; Electron Microscopy Sciences) overnight at 4°C. After cryoprotection in 10%, 20% and 30% sucrose solutions (24 hours in each, at 4°C), the brains

were cut into 30 µm-thick coronal sections using a freezing microtome (Leica SM 2000R). Sections were stored in cryoprotectant solution (30% (v/v) glycerol and 30% (v/v) ethylene glycol in PBS) at -20°C until use.

Sections containing the cingulate cortex (Bregma 1.41 mm to 1.93 mm) and the ventral hippocampus (Bregma -2.91 mm to -3.39 mm) were selected based on the stereotaxic atlas of Paxinos and Franklin (4th edition). We chose these regions, both part of the limbic system, considering their involvement in the regulation of emotional behavior and response to stress (Fanselow and Dong, 2010; McEwen and Gianaros, 2010). For immunofluorescence staining, the free-floating sections were first incubated in citrate buffer [0.1M] at 70°C for 40 min to retrieve antigens. After cooling down, the sections were permeabilized with 0.3% (v/v) H_2O_2 in PBS for 5 min and then washed with PBS. They were then placed in 0.1% $NaBH_4$ solution for 30 min to block non-specific staining and washed. Afterward, the sections were incubated in a blocking solution of 10%(v/v) fetal calf serum with 3% (w/v) bovine serum albumin (BSA) and 0.03% (v/v) Triton X-100 in PBS for 1 hr at room temperature (RT). All primary and secondary antibodies were diluted in blocking buffer. Sections were incubated with anti-IBA1 antibody (ionized calcium-binding adapter molecule 1, 1:150, catalog: MABN92, EMD Millipore) and anti-GR antibody (1:800, catalog: sc-1004, Santa Cruz Biotechnology) at 4°C overnight. Sections were then rinsed in Tris-buffered saline [50mM] (TBS) containing 0.01% (v/v) Triton X-100 (TBS-T), and incubated with a donkey anti-mouse Alexa Fluor ® 488-conjugated (1:300, catalog: A21202, Life Technologies) and a goat anti-rabbit Alexa Fluor ® 568-conjugated (1:300, catalog: A11011, Life Technologies) secondary antibodies for 90 min at RT. Sections were washed in TBS, counter-stained with DAPI (1:20000, Thermo-scientific), mounted on slides and cover-slipped in anti-fading medium (Fluoromount-G, catalog: 0100-01, SouthernBiotech).

Imaging was performed in the cingulate cortex and ventral hippocampal DG polymorphic layer and CA1 *stratum radiatum* (*str rad*) with a Zeiss Axio Imager M2 epifluorescence microscope. The pictures were acquired with an AxioCamMR3 camera (Zeiss, Oberkochen, Germany) using a 20x objective. The analysis of IBA1/GR colocalization was performed blind to the experimental conditions using Photoshop CC 2018 on 2-3 sections/region/animal (n=3-5 animals/experimental group). Every IBA1-positive (+) cell in the pictures in the region of interest was analyzed to assess colocalization with GR in the cell body. For figure presentation, microglial cells were imaged using a Zeiss LSM-880 confocal microscope. Z-stacks were acquired with a 63x objective and the Airyscan module was used for the IBA1 channel. Each stack contained ~95 slices and focus stacking was performed using Zen 3.1 software (Blue edition, Zeiss).

2.3 Chronic unpredictable mild stress (CUMS) paradigm

Following the confirmation of our model, we exposed WT (Cx3cr1CreERT2-/-: Nr3c1fl/fl) and mGR depleted (Cx3cr1CreERT2+/-: Nr3c1fl/fl) female mice treated with tamoxifen to CUMS (n=9-13 animals/group). For the entire duration of the experiment, female mice were housed in the Intellicage system (TSE-system, NewBehavior AG, Zürich, Switzerland), which is an apparatus designed for the automatic monitoring of mouse behavior. It consists of a large acrylic cage (20.5 cm high, 58 cm × 40 cm at the top and 55 cm × 37.5 cm at the base, Model 2000 Tecniplast) with 4 walls separating each corner from the center so that they form 4 identical triangular conditioning chambers (15 × 15 × 21 cm). In this system, animals have access to each chamber by entering a front hole and only a single mouse can enter each chamber at a time since each one is identified by a transponder. The system can collect data about the number and duration of visits and number, duration, and side (right or left) of nose pokes and licks.

The floor of the cage is covered with bedding and contains four sleeping shelters in the center while a food rack on the top is filled with standard mouse chow (food *ad libitum*). One week before being moved to the Intellicage, each animal was injected with a subcutaneous transponder (T-IS 8010 FDX-B; Datamars SA). Mice have been gradually habituated to the Intellicage environment for 14 days. At the same time, they were habituated to drinking a 0.1% saccharin solution for a later assay of taste preferences and motivation.

Standard condition

The standard condition consisted of housing mice in the Intellicage in the absence of stressful procedures. In particular, mice were socially housed in the Intellicage and exposed to Plexiglas shelters of different colours and shapes (four red transparent Tecniplast plastic nest boxes), and to tissue paper. New tissue paper was provided every 5 days and the plastic shelters were cleaned every week.

Stressful condition

After the habituation period, mice were exposed to CUMS procedures to induce depression-like behavior. CUMS lasted three weeks and was expected to induce an approximate 30% decrease of saccharin preference. During CUMS, mice were exposed each day to a different randomly chosen stressor to prevent habituation. The stressors were administered by the Intellicage system, without any physical intervention by the experimenter, and comprised either: Short open door: door to access water or saccharin solution remains open for only 1.5 seconds; Delay: door opens only with a delay of 1, 1.5, 2, 2.5 seconds after the first nosepoke; Open door 25%: door opens only following 25% of nosepokes; Air puff: when the mouse performs a visit, it has a 20% chance to receive an

air puff (2 bar) that lasts 1 s or until the animal leaves the corner and the doors remained closed. During the stressful phase, to drink more, the animals have to leave the corner and start a new visit. The duration of each stressor was randomly 12, 18 or 24 hrs. During the stress-inducing procedures, red LEDs in the corner were turned on when a mouse entered in and turned off at the end of the visit, in order for mice to associate this light condition to the probability of a random stressful event happening. Additionally, during the stressful paradigm, no shelter or tissue paper was provided.

This stressful paradigm, consisting in the constant (24 hrs) exposure of the animals to various stressors, has been previously validated through the assessment of behavioral, cellular, and molecular endpoints (Alboni et al., 2017; Branchi et al., 2013; Poggini et al., 2019). Indeed, the stressful conditions exploited in the present study have been shown to increase basal CORT levels, a marker of stress response in males (Milior et al., 2016).

2.4 Behavioral tests and physiological assessments

The experimental procedures used to phenotype behavior were automatically administered by the Intellicage system, thus avoiding any bias or additional stress due to the presence of experimenter. These included saccharine preference and progressive ratio schedule. In addition, immediately before and at the end of their housing in the Intellicage, the animals were measured for body weight changes. Following the exposure to standard or stressful conditions, plasmatic CORT levels were measured to assess the HPA axis activity and identify potential dysfunctions. Finally, to evaluate the potential association between behavior and hormonal fluctuations, we monitored the estrous cycle of all mice (*see Supplementary Methods*).

Bodyweight

At the end of the habituation period and following the exposure either to the standard or stressful conditions, the bodyweight of the animals was measured at the beginning of the dark phase.

Saccharin preference

To saccharin preference was determined. In each corner of the Intellicage two bottles were present, one containing tap water and the other containing 0.1% saccharin solution; both freely available at all time. Water and saccharin solutions were swapped daily. The position of water and saccharin in each corner was counterbalanced across the four corners. Saccharin preference was determined as follows: (saccharin solution consumed/ saccharin solution consumed + water consumed) × 100. We measured the baseline saccharin preference on the last two days of the habituation period and at the end of the exposure either to the standard or stressful conditions.

Progressive Ratio schedule

To assess the effort to obtaining a reward, we used the progressive ratio reinforcement schedule that utilizes a multiplicative increase in the number of responses (i.e., nosepokes) required to dispense a unit of reinforcement (i.e., saccharin). In particular, water was always accessible after one nosepoke while saccharin solution was accessible only after a specific number of nosepokes performed in a given amount of time. Such number increased progressively after each series of 8 visits according to the following scheme: 2, 3, 4, 5, 6, 7, 8, 10, 12, 16, 20, 24. The time to perform the nosepokes was progressively increased according to the required number of nosepokes from two to 24 seconds. Mice were exposed to this task immediately before and after the exposure to the environmental condition (i.e., standard versus CUMS paradigm). To allow mice to recognize

the session period, the three LEDs on the top of each door were switched on. Each test session lasted two days or until mice reached the module with 24 nosepokes. The animals have been trained on the progressive ratio reinforcement schedule during the habituation phase and before the testing in order to assess their learning performance and control differences in cognitive abilities. The parameter considered was the 'breakpoint', defined as the highest number of consecutive nose pokes performed in a single visit to achieve the access to the bottle.

Locomotor activity – Number of corner visits

To assess the homecage locomotor activity, we measured the number of corner visits per day, both during the habituation period and CUMS.

CORT levels

Plasma CORT levels, which follow a marked circadian rhythm, have been assessed at the end of the dark phase when the hormonal levels are lowest and do not differ between males and females (Lightman and Conway-Campbell, 2010), were measured in all animals at the end of behavioral assessment. In unanesthetized animals, blood was collected from the tail 3 hrs before lights on. The bleeding procedure consisted of a small and superficial cut on the tail. Blood samples were collected individually in potassium–ethylenediaminetetraacetic acid (EDTA) coated 10ml tubes (1.6mg EDTA/ml blood: Sarstedt). All samples were kept on ice and later centrifuged at 3000 rpm for 15 min at 4 °C. Blood plasma was transferred to Eppendorf tubes for CORT determination and stored at -80 °C until analysis. Plasma CORT levels were quantified by enzyme immunoassay according to the manufacturer's recommendations (Corticosterone Elisa kit, Enzo Life Sciences). Samples were diluted 1:40 before analysis, and data were analyzed by sigmoidal 4-parameter

logistic curve fit using Prism 6 (Graphpad). The sensitivity of the assay was 27.0 pg/ml and the intra-assay percent coefficients of variations were between 3.35% and 3.82%.

2.5 Immunohistochemistry staining

Hippocampal adult neurogenesis

24 hrs after the end of the Intellicage paradigm, a cohort of animals was anesthetized with ketamine [80mg/kg]/xylazine [10mg/kg] and perfused transcardially with 4% PFA to assess hippocampal neurogenesis. Brains were post-fixed in 4% PFA overnight at 4°C and cryoprotected in 10%, 20% and 30% sucrose solution (24 hr each concentration). The brains were divided into the hemispheres, right hemispheres were cryoprotected with 30% sucrose, frozen and cut into 40 µm-thick horizontal sections using a manual microtome (HM 430 Sliding Microtome); series of every 8th section were collected and stored in cryoprotection solution (30 %(v/v) glycerol and 30%(v/v) ethylene glycol in PBS) at -20°C until further processing. Sequential horizontal sections containing the hippocampus across the mouse brain (every ~320µm, ~8-9 sections per mice) were collected, mounted in the correct anatomical order and Giemsa-stained (Giemsa stock solution 1.09204.0500, Merck, Darmstadt, Germany). The stained sections were differentiated 10 seconds in 1% acetic acid, dehydrated and coverslipped. For the neurogenesis assessment, free-floating sections were heat-treated for 40 min in citrate buffer (Target Retrieval Solution, DAKO; 1:10, pH 6.0) for epitope retrieval. After pre-incubation in 2% normal serum with 0.25% Triton in TBS for 1 hr at RT, the sections were incubated overnight at 4°C with primary antibodies against Ki-67 (1:300, polyclonal Mouse-anti-Ki-67, BD Pharming) or doublecortin (DCX) (1:2000, Rabbit polyclonal DCX, Abcam ab18723). Incubation in secondary antibody (1:300 for Ki-67 and 1:1000 for DCX) was followed by a 1hr incubation with avidin-biotin complex (ABC) solution (Vectastain). Finally,

sections were stained with 3,3'-diaminobenzidine (DAB) and mounted. DCX stained sections were counterstained with hematoxylin solution and all sections were dehydrated and coversliped.

The total number of DCX+ cells was estimated in the polymorphic layer of the DG with the optical fractionator using the Stereoinvestigator software (MicroBrightField Inc. Williston, USA) with a 63x oil-immersion lens (ZEISS Plan-Apochromat 63x/1.40 Oil DIC). Cells were counted in a frame of 35 µm x 35 µm with x- and y- step sizes of 75 µm. Total cell numbers (N) were calculated using the formula: $N = \sum Q\text{-} \cdot 1\ asf \cdot 1\ ssf$ where ∑Q is the total number of cells counted, *asf* is the area sampling fraction and *ssf* the section sampling fraction. All Ki-67+ cells were counted manually, stained cells in the top focal plane were not considered to prevent over-estimation. Total cell number estimates were calculated by multiplying the cell counts by the section sampling fraction.

Microglial density, distribution and morphology

For the analysis of microglial density, spacing and morphology, ventral hippocampal sections (Bregma -2.91 mm to -3.39 mm) were incubated in citrate buffer at 70°C for 40 min for antigen retrieval. After the sections had cooled down, the free-floating sections were placed in 0.1% $NaBH_4$ solution for 30 min and washed. They were incubated in a blocking solution of 10% donkey serum with 0.5% gelatin and 0.1% Triton X-100 in PBS for 1 hr at RT. Sections were then incubated with anti-IBA1 (1:150, catalog: MABN92, EMD Millipore) and anti-TMEM119 (Transmembrane Protein 119) (1:300, catalog: ab209064, Abcam) antibodies at 4°C overnight, rinsed in PBS(T) 0.01%, and then incubated with an Alexa Fluor ® 555-conjugated (1:300, catalog: A31570, Invitrogen) and an Alexa Fluor ® 647-conjugated (1:300, catalog: A31573, Invitrogen) secondary antibodies for 90 min at RT. All primary and secondary antibodies were

diluted in the same blocking buffer. Sections were washed in PBS, counter-stained with DAPI (1:20000, Thermo-scientific), mounted on slides, then coverslipped with anti-fading medium (Fluoromount-G, SouthernBiotech).

6 sections/mice in 6 mice per experimental group were used for imaging. For density, distribution and infiltration analyses, sections containing the hippocampal DG polymorphic layer and CA1 *str rad* were imaged in a single plane at 20x magnification using an Axio Imager M2 epifluorescence microscope equipped with an AxioCamMR3 camera (Zeiss, Oberkochen, Germany) and mosaics were created with Zen 3.1 software (Blue edition, Zeiss). For the morphological analysis, the hippocampal DG polymorphic layer and CA1 *str rad* were imaged using a Quorum WaveFX Spinning disc confocal microscope. Z-stacks were acquired with a 20x objective and an ORCA-R2 camera (Hamamatsu, 512 x 512 pixels). Each stack contained ~30 slices (1µm each) and focus stacking was performed using Volocity software (Version 5.4, PerkinElmer).

Microglial density, spacing, and morphology were analyzed in all the captured images from the 6 sections/mice in 6 mice per experimental group. The analysis was performed blind to the experimental conditions with ImageJ software (National Institutes of Health) as previously described (Tremblay et al., 2012). Density and spacing were calculated, respectively, using the "analyze particles" and "nearest neighbour distance" plugins of ImageJ. Cellular density was defined as the total number of cells divided by the total area (cells/mm^2) for each region of interest in each animal. Spacing index was calculated as the square of the average nearest neighbour distance (NND) multiplied by microglial density per region of interest and animal. For the infiltration analysis, total counts of IBA1+/TMEM119+ (microglia) and IBA1+/TMEM119 negative (-) (peripheral/perivascular macrophages) cells were compiled per region of interest and

animal, using the analyze particles plugin (Ibanez González et al., 2019). Morphology was analyzed for 15-20 microglial cells per animal, selected based on their complete visualization. Soma and arborization areas were determined using the "drawing" and "measure" tools in ImageJ and converted in µm². A morphological index was then determined using the formula: soma area/arborization area was also compiled (Ibanez González et al., 2019; Tremblay et al., 2012). The larger the value, the greater the soma size was in relation to the arbor size. Circularity and solidity were next determined using the shape descriptors plugins in ImageJ as described in Bordeleau *et al*, 2020 (Bordeleau et al., 2020). Briefly, circularity was calculated by: $4\pi\times(\text{Area}/\text{Perimeter}^2)$ for which a value of 1.0 represent a perfect circle. Solidity was calculated by dividing the cell area by the convex cell area for which a value closer to 1.0 indicates a more convex shape.

2.6 Isolation of CD11b⁺ cells from hippocampus and real-time polymerase chain reaction

Hippocampus of mice previously perfused with saline to eliminate circulating peripheral immune cells were cut into small pieces and single-cell suspension was achieved in Hank's balanced salt solution (HBSS). The tissue was further mechanically dissociated using a glass wide-tipped pipette and processed for cluster of differentiation (CD)11b+ cells extraction with a magnetic-activated cell sorting (MACS) system (Garofalo et al., 2017). Briefly, CD11b+ cells were magnetically labelled with CD11b MicroBeads and the cell suspension was loaded onto a MACS Column placed in the magnetic field of a MACS Separator. CD11b+ cells were eluted as the positive fraction. Live CD11b+ cells were assessed by flow cytometry and the purity was ~99% (Garofalo et al., 2017).

RNA was isolated with the RNeasy Mini Kit and processed for real-time polymerase chain reaction (rt-PCR) (Qiagen) in duplicate, and the intra-assay coefficient of variation was below 30%. The quality and yield of RNAs were verified using the NANODROP One system (Thermo Scientific). Reverse transcription reaction of CD11b+ cells collected by MACS was performed in a thermocycler (MJ Mini Personal Thermal Cycler; Biorad) using IScript TM Reverse Transcription Supermix (Biorad) according to the manufacturer's protocol, under the following conditions: incubation at 25°C for 5 min, reverse transcription at 42°C for 30 min, inactivation at 85°C for 5 min. rt-PCR was carried out in a I-Cycler IQ Multicolor rt-PCR Detection System (Biorad) using SsoFast EvaGreen Supermix (Biorad) according to the manufacturer's instructions. The PCR protocol consisted of 40 cycles of denaturation at 95°C for 30 s and annealing/extension at 60°C for 30 s. For quantification analysis, the comparative cycle threshold (Ct) method was used. The ΔCt was calculated by the difference between Ct values of each gene of interest and the Ct value of glyceraldehyde 3-phosphate dehydrogenase (GAPDH), then normalized with the non-stressed WT group (reference group) to obtain the ΔΔCt. Relative quantification was performed using the $2^{\Delta\Delta}C_t$ method and expressed as fold change in arbitrary values. The primers used are listed in Table 1.

2.7 Electrophysiology

Extracellular field recordings

Animals were anesthetized by inhalation of halothane (Sigma-Aldrich) and then decapitated. The whole brain was rapidly removed from the skull and immersed in ice-cold artificial cerebrospinal fluid (ACSF) solution containing (in mM): NaCl 125, KCl 4.4, $CaCl_2$ 2.5, $MgSO_4$ 1.5, $NaH2PO_4$

1, $NaHCO_3$ 26 and glucose 10. ACSF was continuously oxygenated with 95% O_2 + 5% CO_2 to maintain a pH close to 7.4. Following removal, the brain tissues were blocked on the stage of a vibrating microtome (Thermo Scientific) and 350 μm thick slices were cut in ice-cold ACSF. The hippocampal slices were then transferred to an incubation chamber containing oxygenated ACSF, where they recovered for 1 hr at 30 °C prior to field recording. Individual slices were then transferred to an interface slice-recording chamber (BSC1, Scientific System Design Inc) with a total fluid dead space of about 3 ml, to perform experiments within 1–6 hrs after slice preparation. They were maintained at 30–32 °C and constantly superfused with ACSF at the rate of 2 ml/min using a peristaltic pump. A concentric bipolar stimulating electrode (SNE-100 × 50mm long, Elektronik–Harvard Apparatus GmbH) was placed in the CA1 *str rad* to stimulate Schaffer collateral fibers. Stimuli consisted of 100 μs constant current pulses of variable intensity, applied at 0.05 Hz. An ACSF-filled glass micropipette (0.5–1 MΩ) was placed in the CA1 region, at 200–600 μm from the stimulating electrode, in order to measure orthodromically-evoked field extracellular postsynaptic potentials (fEPSP). Stimulus intensity was adjusted to evoke fEPSPs of amplitude about 50% of maximal amplitude with minimal contamination by a population spike. Evoked responses were monitored online, and stable baseline responses were recorded for at least 10 min. Only the slices that showed stable fEPSP amplitudes were included in the experiments. LTP was induced by high-frequency stimulation (HFS, 1 train of stimuli at 100 Hz, of 1 s duration). To analyze the time course of fEPSP amplitude, the recorded fEPSP was routinely averaged over 1 min (n = 3). fEPSP amplitude changes following the LTP induction protocol were calculated with respect to the baseline.

fEPSPs were recorded and filtered (low pass at 1 kHz) with an Axopatch 200 A amplifier (Axon Instruments, CA) and digitized at 10 kHz with an A/D converter (Digidata 1322 A, Axon

Instruments). Data acquisition was stored on a computer using pClamp 9 software (Axon Instruments) and analyzed off-line with Clampfit 10 program (Axon Instruments).

Patch-clamp recordings

Patch clamp recordings were performed as described in Basilico *et al.*, 2019 (Basilico et al., 2019). Briefly, animals were decapitated under halothane anesthesia. Whole brains were removed and immersed for 10 min in ice-cold ACSF solution containing (in mM): KCl 2.5, $CaCl_2$ 2.4, $MgCl_2$ 1.2, $NaHPO_4$ 1.2, glucose 11, $NaHCO_3$ 26, glycerol 250. The ACSF was continuously oxygenated with 95% O_2 and 5% CO_2 to maintain the physiological pH. Horizontal 250 µm thick hippocampal slices were cut at 4°C, using a Vibratome (DSK, Dosaka EM), and placed in a chamber filled with oxygenated ACSF containing (in mM): NaCl 125, KCl 2.5, $CaCl_2$ 2, $MgCl_2$ 1, $NaHPO_4$ 1.2, $NaHCO_3$ 26 and glucose 10. Before use, slices were allowed to recover for at least 1 hr at RT. All recordings were performed at RT on slices submerged in ACSF and perfused with the same solution in the recording chamber.

Evoked excitatory postsynaptic currents (EPSC) were recorded from CA1 pyramidal neurons using the patch-clamp technique in whole-cell configuration at -70 mV. Patch pipettes (3-5 MΩ) were filled with intracellular solution containing (in mM): Cs-methanesulfonate 135, HEPES 10, MgATP 2, NaGTP 0.3, $CaCl_2$ 0.4, $MgCl_2$ 2, QX-314 2, BAPTA 5 (pH adjusted to 7.3 with CsOH). Bicuculline methochloride (10 µM) was added to extracellular solution to block $GABA_A$ receptors. EPSC were evoked by electrical stimulation with theta glass tubes filled with external solution. Stimulating electrodes were connected to the stimulus isolation unit (Iso-stim A320, WPI) and placed in the *str rad*, 100-150 µm from the patched CA1 neuron, to activate the Schaffer collaterals projecting to CA1. Synaptic responses were evoked by stimulating for 100 µs at 0.1 Hz, the

stimulus intensity was adjusted accordingly to the experiment. AMPA-mediated EPSC were evoked by paired-pulse stimulations (interval 50 ms) to determine the paired-pulse ratio (PPR), calculated as the ratio between the amplitude evoked by the second stimulus (A2) over the first (A1; A2/A1). The input/output (I/O) of the AMPA component was determined at -70 mV, stimulating Schaffer collaterals at increasing intensities (0.1 - 10 mA). Each pulse of a given intensity was repeated 6 times to obtain an average response. To determine the AMPA/NMDA ratio, stimulus strength was adjusted to obtain at -70 mV stable AMPA-mediated EPSC with an amplitude corresponding to the 50% of the maximum response. The NMDA current was recorded at +40 mV from the same neuron, using the same stimulus strength. During the analysis, NMDA peak amplitude was measured with a delay of 25 ms from the AMPA peak. Recordings were made with a patch-clamp amplifier (Axopatch 200A, Molecular Devices), filtered at 2 kHz, digitized (10 kHz) and acquired using pClamp 10.0 software (Molecular Devices); the analysis was performed off-line using Clampfit 10 (Molecular Devices).

2.7 Statistical analyses

For GR microglial deficiency characterization and microglial analyses (density, distribution, morphology), as well as peripheral/perivascular myeloid cells, statistical analyses were conducted using 2-way ANOVA with the software Prism (GraphPad, Version 8). *Post-hoc* comparisons were performed using Bonferroni's correction for GR microglial deficiency characterization to compare the other groups to the WT oil group and Tukey's correction for the microglial analyses. Sample size (n) refers to the number of animals in each experiment, except for the microglial morphology analysis where it refers to the cell number, as previously conducted by our group (Hui et al., 2018; Lecours et al., 2020; Milior et al., 2016). Intellicage, neurogenesis and electrophysiological

experiments were analyzed with 2-way ANOVAs with the software Statview II (Abacus Concepts) or R and Sigmaplot software, considering genotype (WT and microglial-GR depletion) and environmental condition (standard, stress) as the between-subject variables. *Post-hoc* comparisons were performed using Tukey's correction (Milior et al., 2016). Microglial gene expression data were tested for equal variances and then analyzed with 2-way ANOVAs with Sigmaplot software and *post-hoc* comparisons were performed using Holm-Sidak's correction. All mean differences were considered statistically significant when $p < 0.05$. All reported values are mean ± standard error of the mean (SEM).

3 Results

We investigated the effects of microglial-GR depletion on microglia and neuronal circuits, at steady-state and in response to CUMS using female mice, considering that they are more vulnerable to chronic stress and have a higher predisposition to stress-induced anxiety and depression compared with males (Heck and Handa, 2019). The animals were habituated to the Intellicage system for two weeks, and then exposed to a stressful (CUMS) or standard (without stress) housing environment for three additional weeks (Figure 1). After sacrifice of the animals, cellular, molecular and electrophysiological analyses were performed in the hippocampal CA1 *str rad* and the DG polymorphic layer, two key regions involved in the adaptation to stress (McEwen, 2001).

3.1 The microglial-GR depletion mouse model almost completely suppresses microglial GR expression

To characterize our mouse model, we first verified that microglia were depleted for GR in both male and female mice using a double immunofluorescent staining against the microglial marker IBA1 and GR. The observations were made in the cingulate cortex, CA1 *str rad* and DG polymorphic layer of WT *versus* mGR depleted animals that received either tamoxifen to induce microglial-GR deletion or oil as a control. In mGR depleted female mice, we observed a significant decrease in the proportion of microglia expressing GR following tamoxifen administration in the three regions compared to the WT oil group (Figure 2), the cingulate cortex (78.05 ± 2.19 % (WT oil) *vs* 6.17 ± 1.64% (mGR depletion Tam) [$F_{(1,9)}$=553.9, p<0.0001]) (Supplementary Figure 1a), the CA1 *str rad* (78.13 ± 1.09% (WT oil) *vs* 4.54 ± 2.28 % (mGR depletion Tam) [$F_{(1,9)}$=482.0, p<0.0001]) and DG polymorphic layer (97.78 ± 0.48 % (WT oil) *vs* 4.44 ± 4.44 % (mGR depletion Tam) [$F_{(1,9)}$=126.7, p<0.0001]) (Figure 2). The same decrease was observed in males in the cingulate cortex (80.50 ± 2.16 % (WT oil) *vs* 5.91 ± 0.10 % (mGR depletion Tam) [$F_{(1,10)}$=204.3, p<0.0001]) and the CA1 *str rad* (78.17 ± 0.77 % (WT oil) *vs* 4.17 ± 0.21 % (mGR depletion Tam) [$F_{(1,11)}$=328.4, p<0.0001]) (Supplementary Figure 1b-c). The tamoxifen treatment did not induce a complete depletion, which is consistent with what was previously observed in other models of tamoxifen-induced depletion in microglia (Goldmann et al., 2013). Tamoxifen *versus* oil also induced a moderate increase in microglial GR expression in the female WT animals, among the CA1 *str rad* (78.13 ± 1.09 % (WT oil) *vs* 91.10 ± 2.34 % (WT Tam) [$F_{(1,9)}$=482.0, p<0.0001]) and theccingulate cortex (78.05 ± 2.19 % (WT oil) *vs* 92.05 ± 1.73 % (WT Tam) [$F_{(1,9)}$ =482.0, p<0.0001]).

3.2 CUMS affects the neurobehavioral profile independently from the genetic background

At the end of the habituation period, we measured the bodyweight of the animals and we did not observe a significant difference between the genotypes [$F_{(1,41)}$ =0.224, p=0.6386] (Figure 3a). At

the end of the experiment, we calculated the difference of body weight between before and after the exposure to the different conditions. We observed a significant effect of stress exposure, with both mGR depleted and WT mice exposed to CUMS showing a significant reduction of body weight compared to the animals in standard condition [$F_{(1,38)}$ =100.7, p<0.0001] (Figure 3b). The increase in basal peripheral CORT levels after CUMS failed to reach statistical significance [$F_{(1,32)}$ =2.139, p=0.153] (Figure 3c).

When we assessed the saccharine preference on the last two days of habituation, immediately before the animals were exposed to the standard or stressful paradigms, both mGR depleted and WT mice showed a strong preference for the saccharin solution [$F_{(1,41)}$ =3.990, p=0.0524] (Figure 3d). Following the exposure to the standard condition, both genotypes maintained a clear preference for the saccharin solution. By contrast, the exposure to the CUMS induced a significant decrease of saccharine preference, with no difference between mGR depleted and WT animals [$F_{(1,38)}$ =15.00, p <0.0001] (Figure 3e).

During the habituation phase, WT and mGR depleted mice were trained to progressive ratio. During training, they did not differ in the breakpoint reached [$F_{(1,41)}$=1.843, p=0.1821], suggesting that the depletion of the microglial GR does not impair associative learning. During the first progressive ratio aimed at assessing the motivation response, immediately before stress, no difference in the breakpoint reached between mGR depleted and WT mice was found [$F_{(1,39)}$=3.383, p=0.0735] (Figure 3f). As expected, CUMS significantly affected the anhedonic response, stressed mice showing a significantly lower breakpoint compared to animals exposed to standard condition [$F_{(1,37)}$=7.612, p=0.0090]. No interaction effect between genotype and condition was found [$F_{(1,37)}$=6.456, p=0.9936] (Figure 3g).

Finally, we investigated the locomotor activity of the animals as measured by the number of corner visits per day. We did not observe an effect of genotype on activity neither during the habituation period nor the stress exposure (data not shown).

All the neurobehavioral parameters assessed were not affected by the estrous cycle (data not shown).

3.3 Microglial-GR depletion affects microglial morphology in a region-specific manner

To provide insights into the consequences of microglial GR depletion on brain immunity, we next evaluated microglial density and distribution, as well as perivascular and infiltrating peripheral myeloid cells, in the CA1 *str rad* and the DG polymorphic layer using a double immunofluorescent staining against IBA1 (labels all myeloid cells including microglia) and TMEM119 (specific to microglia). We found that microglial density, NND and spacing index (compiling the average nearest neighbour and microglial density) (Figure 4), as well as perivascular and infiltrating peripheral myeloid cells (proportion of cells only IBA1+) (Table 2) were not modified by CUMS or microglial GR deficiency in both regions.

In the CA1 *str rad*, microglial arborization area increased with CUMS in WT animals (2278 ± 76.83 μm^2 *vs* 2705 ± 72.77 μm^2, p=0.0013; Figure 5c). However, this increase was not observed with CUMS in mGR depleted animals (2714 ± 95.31 μm^2 *vs* 2616 ± 79.96 μm^2). In agreement with this result, microglial morphological index (soma area/arborization area) was significantly decreased following stress in WT animals (0.0314 ± 0.0013 a.u *vs* 0.0263 ± 0.0009 a.u., p=0.0056; Figure 5d), but not in mGR depleted animals (0.0284± 0.0010 a.u. *vs* 0.0289 ± 0.0012 a.u.). Microglial arborizations were also larger in mGR depleted animals compared to WT animals in

standard housing condition (2713.918 ± 95.305 µm^2 *vs* 2277.628 ± 76.828 µm^2, $p = 0.0011$; Figure 5c). Microglial morphology did not differ significantly between genotypes and environmental conditions in the DG polymorphic layer (Figure 5 g, h and Table 2).

3.4 Microglial-GR depletion affects microglial inflammatory gene expression upon CUMS

To determine if GR deficiency modulated microglial inflammatory phenotype at steady-state and upon CUMS, we sorted microglial (CD11b+) cells from hippocampus of mGR depleted or WT mice and analyzed the expression of different pro- or anti-inflammatory genes and of genes involved in microglial homeostatic functions (Triggering receptor expressed on myeloid cells 2 (*Trem2*), myeloid-epithelial-reproductive tyrosine kinase (*Mertk*) and *Cx3cr1*). In standard condition, mGR depleted-microglia expressed higher levels of pro-inflammatory genes (*Il1b* and tumor necrosis factor α (*Tnfa*)) (Figure 6b, c), and increased the expression of genes involved in phagocytic activity and in the modeling of synaptic transmission (cluster of differentiation *Cd68, Trem2*, *Mertk* and *Cx3cr1*) (Figure 6a, g, h, i). Furthermore, CUMS increased the expression of anti-inflammatory genes (*Arg-1* and *Fizz-1*) (Figure 6d, e) in mGR depleted *vs* WT microglia, and reduced the expression of pro-inflammatory (*Tnfa*), phagocytic (*Cd68)* as well as other functional (*Trem2*, *Mertk* and *Cx3cr1*) genes (Figure 6). There was no change in *Bdnf* (Brain-derived neurotrophic factor).

3.5 Microglial GR deficiency alters adult hippocampal neurogenesis

Microglia are known to influence adult hippocampal neurogenesis and this interaction can be affected by chronic stress (Sierra et al., 2014). To evaluate whether the microglial GR deficiency had an impact on this neurogenesis, we used immunochemistry against Ki-67 (a marker of proliferating cells) and DCX (a marker of newborn neurons). The analysis of Ki-67+ cells density

revealed that the exposure to either standard or stressful conditions does not affect proliferation [$F_{(1,16)}$=0.637, p=0.4363] (Figure 7a). By contrast, DCX+ cells density was affected by the genotype [$F_{(1,15)}$=5.888, p=0.0283], but no interaction was found [$F_{(1,15)}$=1.725 p=0.20875]. *Post-hoc* analysis revealed that, in the standard condition, DCX+ cells number is significantly increased in mGR depleted mice compared to WT (Figure 7b), suggesting an increased number of immature neurons (p <0.05). Exposure to CUMS led to the normalization of adult neurogenesis: mGR depleted mice exposed to stress showed a similar number of DCX+ cells as in WT mice exposed to standard conditions.

3.6 Microglial GR deficiency affects CA1 hippocampal plasticity, increasing sensitivity to stress

To investigate the effect of microglial GR gene depletion on hippocampal plasticity processes, we explored CA1 plasticity inducing long-term potentiation (LTP) by a single Schaffer collateral stimulation (1 train of stimuli at 100 Hz) in WT and mGR depleted mice exposed to standard or stressful conditions. Notably, in WT mice, exposure to stress did not produce any effect, whereas it reduced the amplitude of LTP in mGR depleted mice. An interaction between genotype and environmental condition additionally emerged [$F_{(1,53)}$=4.958, p=0.0300]. In particular, *post-hoc* analysis revealed that under standard condition, the experimental groups did not differ in their LTP amplitude (WT, 1.499±0.044; mGR depletion, 1.547±0.0390) (Figure 8a) but in stressful condition, mGR depleted mice showed a significant decrease in LTP amplitude (1.413±0.038) compared to both mGR depleted and WT mice in standard condition (p=0.018) (Figure 8a) and to stressed WT mice (1.539±0.036, p=0.0396).

By means of patch-clamp recordings, we measured the PPR, a form of short-term plasticity related to neurotransmitter release probability (Zucker, 1989). We determined the ratio between the

amplitude evoked by a second stimulus over the first, by stimulating the Schaffer collaterals projections to CA1 at 50 ms intervals. As shown in Figure 8b, in WT mice, stress did not modify PPR value, by contrast, it significantly reduced the value in the mGR depleted. We found an effect of genotype in stress condition (p=0.0260) and *post-hoc* analysis showed that in mGR depleted mice, exposure to stress reduced PPR value (1.027±0.115) compared to the standard housing condition (1.552±0.151, p=0.0080).

3.7 Microglial GR deficiency affects hippocampal synaptic connectivity independently of stress

We stimulated the CA1 Schaffer collaterals using a graded stimulation and recorded the resulting AMPA responses. As shown in Figure 8c, we compared I/O curves between genotypes exposed to different environmental stimuli. We observed that overall WT mice at different stimulus intensity displayed a significantly weaker peak currents compared to mGR depleted mice [$F_{(1,253)}$=7.533, p=0.0070] in both environmental conditions, indicating that in the absence of GR, hippocampal synapses showed higher synaptic connectivity compared to WT mice.

We then measured the amplitude of AMPA receptor (AMPAR) and NMDA receptor (NMDAR)-mediated components of postsynaptic currents at -70 mV and +40 mV of holding potential, respectively, to determine AMPA/NMDA ratio (Hoshiko et al., 2012). This ratio evaluated in WT and mGR depleted mice did not differ between experimental conditions (Figure 8d).

4 Discussion

In the present study, we developed a depletion model of microglial GR inducible by tamoxifen during adulthood. Using that model, we show that microglial GCs-GR signaling plays an important

role in modulating microglial phenotype and hippocampal plasticity in both standard and stressful conditions. Indeed, mGR depleted mice had an increased microglial arborization and higher number of newborn cells, as well as an increased expression of microglial gene-related to synaptic plasticity and inflammation. Moreover, contrary to WT mice, mGR depleted mice exposed to CUMS had a decreased LTP and PPR and their microglia displayed a shift towards an anti-inflammatory gene profile. Behavioral characterization further revealed that CUMS induced a decrease of both saccharine preference and progressive ratio breakpoint, suggesting stress-related behaviors that are not prevented by the mGR depletion. However, it is possible that GR depletion affected other behaviors involving the corticolimbic regions that we did not test, such as the anxiety (Wohleb, 2016).

Tamoxifen induced a moderate increase in microglial GR expression in the female WT animals compared to vehicle controls. This increase might relate to tamoxifen's modulation of estrogen receptors (Singh et al., 2008), which are known to be expressed by microglia (Sierra et al., 2008) and to interact with GR (Vahrenkamp et al., 2018). Moreover, estradiol is known to possess a protective effect against some of the deleterious effects of stress (e.g., synaptic transmission impairments, dendritic atrophy) (Garrett and Wellman, 2009; Wei et al., 2014), a phenomenon that might be prevented by tamoxifen considering its anti-estrogenic properties (Singh et al., 2008). To consider these possible effects of tamoxifen, all of our animals exposed to standard or CUMS environments did receive tamoxifen, including WT groups. While tamoxifen may have altered baseline responses of the outcomes measured, and may interact with CUMS, we observed differences between the WT and mGR depleted groups, pointing to a role of microglial GR in modulating these reactions to CUMS. Nevertheless, replicating an equivalent microglia-specific

depleted model using a different approach would shed more light onto the possible effects of tamoxifen.

4.1 Microglial-GR signaling deficiency alters microglial and neuronal properties at steady-state

Our results demonstrate that the microglial GR plays an important role in modulating microglial functions under normal homeostatic conditions. Indeed, microglia from mGR depleted mice differed from those of WT mice by showing an increased arborizations in the CA1 *str rad* while no difference was observed in the DG polymorphic layer. The morphology of GR-deficient microglia was previously characterized by Carrillo-de Sauvage *et al* using $GR^{LysMCre}$ mutant mice in which both microglia and peripheral macrophages were conditionally deficient in GR. They did not observe differences in the microglial surface area within the cerebral cortex under normal physiological conditions (Carrillo-de Sauvage et al., 2013). Thus, the observed increase of microglial arborization that we measured could be specific to the CA1 *str rad.* This is consistent with the known heterogeneity of microglia between brain regions (Tan et al., 2020). The increased microglial arborizations area was associated with an increase in microglial gene expression of *Mertk*, which can regulate microglial process surveillance and phagocytosis (Fourgeaud et al., 2016), and an increase of *Cd68* that is associated with phagolysosomal activity (Lecours et al., 2020). This could indicate a higher activity of microglia notably in extracellular debris clearance and synaptic remodeling (Lecours et al., 2020). Moreover, GR depleted microglia had increased gene expression of *Cx3cr1* and *Trem2*, both involved in microglial migration, phagocytosis and remodeling of synaptic transmission (Castro-Sánchez et al., 2019; Filipello et al., 2018; Maggi et al., 2011; Mazaheri et al., 2017). These results suggest that GR depleted microglia might be more involved in synaptic plasticity, and that microglial GR has a role in maintaining microglia in a

surveillant state. However, the physiological and functional changes associated with microglial hyper-ramification are still not well understood and warrant further investigation.

Consistent with their homeostatic microglial functional changes, mGR depleted mice presented an alteration in the hippocampal synaptic connectivity at steady state. Higher AMPA I/O curves in the mGR depleted compared to the WT mice were measured after stimulation of the Schaffer collaterals, and could be explain by a higher number of functional synapses. This could be linked with the increased microglial *Tnfa* we observed in the mGR depleted mice. Indeed, it was shown that glial *Tnfa* promotes the expression of AMPA glutamate receptors in neurons (Stellwagen et al., 2005; Stellwagen and Malenka, 2006). Another potential cause behind the neuronal connectivity change could be the increased number of DCX+ cells in mGR depleted mice compared to the WT mice. Microglia play a key role in the regulation of neurogenesis by phagocytosing the excess of newborn cells (Sierra et al., 2010) and releasing neurotrophic factors such as insulin-like growth factor 1 (IGF-1) that promote neurogenesis (Gemma and Bachstetter, 2013). Considering the increase of microglial *Mertk* and *Cd68*, the observed increase in newly generated cells did not likely result from a deficit in microglial phagocytic engulfment of newborn cells (Fourgeaud et al., 2016). Instead, it could arise from a decreased microglial release of trophic factors (e.g., IL-7, IL-11) that can promote their differentiation (Sierra et al., 2014). These effects could also be mediated by the increase in *Cx3cr1*, which is known to be involved in hippocampal neurogenesis. Indeed, male mice deficient in CX3CR1 presented a decrease in hippocampal neurogenesis (Bachstetter et al., 2011), as well as in the functional connectivity (Basilico et al., 2019), which suggests an implication of the receptor in this process. It has been widely reported that elevated levels of GCs reduce adult hippocampal neurogenesis, inhibiting cell proliferation, differentiation, and survival (Bessa et al., 2009; Egeland et al., 2015; Gould et al., 1998; Morais et

al., 2014). Notwithstanding, knowledge into the role of microglial GRs in these neurogenic processes, including cellular proliferation and differentiation, remains limited. Nevertheless, the high expression of GR on microglia suggests that GCs can affect neurogenesis via both neuronal and microglial GRs.

Microglia deficient in GR additionally presented at steady-state an increased expression of *Il1b* and *Tnfa*, which are considered to be pro-inflammatory cytokines (Liu and Quan, 2018). At steady-state, GR is known to promote anti-inflammatory actions through its inhibition of the transcription of pro-inflammatory genes (Escoter-Torres et al., 2019). Thus, its absence could induce the transcription of inflammatory genes that have normally been inhibited, with possible consequences on the mechanisms underlying the response of the brain to environmental challenges such as CUMS.

4.2 Role of microglial GCs-GR signaling in response to CUMS

The main finding of our study is that the impairment of microglial GCs-GR signaling leads to an alteration of microglial morphology and gene profile, as well as synaptic plasticity (LTP and PPR), but does not affect the behavioral response to CUMS exposure. The CUMS paradigm did not induce a significant increase in CORT, which could be due to sex differences. Studies of HPA axis dysregulation in rodent depression models reports that CORT is not always increased in females as it is in males. In a chronic isolation/restrain model, the stress resulted in increased adrenocorticotropic hormone levels, without changes in CORT levels in female mice (Dong et al., 2020). Another study using foot-shock stress revealed a higher CORT increase in socially-isolated male compared to female rats (Pisu et al., 2016).

In terms of microglial changes, CUMS did not modify density in the CA1 *str rad* or the DG polymorphic layer in both genotypes. There was very marginal myeloid cell infiltration, only observed in the stress condition in both genotypes. This is consistent with studies showing chronic stress can promote the recruitment of peripheral cells in males and female mice, although this was observed in a repeated social defeat paradigm (Weber et al., 2019; Yin et al., 2019), which is a stronger, more physical stressor (Golden et al., 2011). We also found that WT animals had an increase in the microglial arborizations area in the CA1 *str rad*, but not in the DG polymorphic layer. Microglial hyper-ramification following chronic stress was previously observed in the DG in mice (Hellwig et al., 2016), as well as in the medial prefrontal cortex (mPFC) (Hinwood et al., 2013, 2012) and CA3 of rats (Franklin et al., 2018). However, some studies reported a decrease in microglial arborization in CA1 *str rad* of male mice following CUMS (Milior et al., 2016) or de-ramification in the mPFC (Horchar and Wohleb, 2019), medial amygdala, paraventricular nucleus, DG and hippocampus of male mice following repeated social defeat (Wohleb et al., 2014a, 2014b, 2011). These different results could be due to a myriad of factors including the stress paradigms and their duration, the sex, and the brain regions studied. In fact, it is widely documented that varied stress models have profoundly different effects on neuroimmune function as well as behavior (Deak et al., 2015; Patchev and Patchev, 2006; Picard et al., 2021), which further highlights the complexity and context-dependent nature of the stress response.

Interestingly, the lack of microglial GCs-GR signaling impaired the microglial morphological response to CUMS in the CA1 *str rad*. Hippocampal microglial hyper-ramification was proposed to be induced by an increase of GCs signaling. Van Olst *et al* showed that enhancing GCs levels using slow-release GC pellets in adult male mice directly increased CD11b immunolabeling and microglial ramifications in the molecular layer of the DG (Olst et al., 2018). This work showed a

relationship wherein administration of GCs alters microglial morphology, albeit directly test whether this was through microglial GR; wherein, conversely, our works shows that an absence of microglial GR impaired microglial morphological response to CUMS. Our results are also in line with a recent study by Horchar and Wohleb, which demonstrated that administration of an antagonist of GR (RU486) limited the microglial morphological alterations in the PFC of male mice undergoing CUMS (Horchar and Wohleb, 2019). Together, this implies both a necessity and sufficiency for GR-GCs interactions to alter microglia morphology in response to chronic stress or repeated CORT exposure. Contrary to our findings, GR blockade prevented chronic stress-induced behavioral despair (Horchar and Wohleb, 2019). This might be due to the fact that RU486 is also an antagonist of progesterone receptors (Cadepond et al., 1997) and can inhibit GR in other cell types of the CNS, including neurons (Sousa et al., 1989), oligodendrocytes, and astrocytes (Vielkind et al., 1990). It is also possible that the microglial modifications we observe do not translate into behavioral changes because they are compensated by other CNS cells. GR in astrocytes was recently shown in male mice to be important for mediating the brain response to GCs, mainly for stress-induced memory formation (Tertil et al., 2018).

Moreover, CUMS induced an increase in microglial *Cd68*, *Il1b* and *Tnfa* gene expression, which is in agreement with previous studies showing an increase in microglial pro-inflammatory cytokines upon exposure to various chronic stress paradigm, such as CUMS (Intellicage) (Alboni et al., 2016) and repeated social defeat (Weber et al., 2019). In contrast, mGR depleted mice exposed to CUMS showed an increased microglial gene expression of *Fizz1* and *Arg1*, both known to have anti-inflammatory functions (Cherry et al., 2014), and a decrease of *Cd68* and *Tnfa*. While microglia are partially insensitive to CORT in mGR depleted mice, they could be responding to

the inflamed microenvironment (Munhoz et al., 2008) caused by chronic stress through other receptors and respond to it by increasing their anti-inflammatory properties.

We did not observe any change in neurogenesis in the DG polymorphic layer following exposure to CUMS for both genotypes, which is in disagreement with previous studies showing a decrease of neurogenesis following CUMS (Eid et al., 2020) and repeated water-immersion and restraint stress (Shimizu et al., 2019) in female mice. However, unlike our study, the mice were ovariectomized in both studies, which supports a putative protective role of estrogen. Moreover, genes involved in the positive regulation of neurogenesis were shown to be upregulated in female mice upon CUMS (Lotan et al., 2018). This gene regulation could protect females from the decrease in neurogenesis often observed in male mice after chronic stress (Ferragud et al., 2010; Mitra et al., 2006; Schloesser et al., 2010).

At the neuronal circuit level, WT controls showed no modification with CUMS exposure, which is in contradiction with the literature showing that hippocampal LTP is impaired after chronic stress (Joëls and Krugers, 2007; Kim and Diamond, 2002). The effects of stress on the neuronal excitability of the female brain remain largely unknown. Only a few studies have been conducted in females and the mechanisms underlying sex differences have not yet been clarified in the context of stress response. It has been reported that chronic stress impairs behavioral responses in the males but not female rats (Lin et al., 2008; Zuena et al., 2008), as well as induces sexual dimorphism in synaptic innervation of hippocampal subiculum (Carvalho-Netto et al., 2011; Jp et al., 2000). Contrary to males, female rats also did not exhibit the same severity of apical dendritic atrophy seen after stress exposure (Galea et al., 1997). Interestingly, CUMS results in a significant decrease in pCREB expression, involved in long-term synaptic plasticity and memory, specifically in male

DG (Lin et al., 2008). These results suggest that females are less susceptible to the aversive effects of chronic stress. Nevertheless, more studies are needed to unravel the mechanisms underlying these important sex differences. Hippocampal LTP is known to be sexually dimorphic under basal conditions, with females having a lower amplitude than males in rats (Monfort et al., 2015). In this regard, our's and other's groups have previously demonstrated that following CUMS in male rodents, hippocampal short and long-term plasticity are impaired (Joëls and Krugers, 2007; Kim and Diamond, 2002; Milior et al., 2016). Here we show for the first time that, following the same environmental paradigm (CUMS), that females do not have reduced cellular hippocampal neuronal plasticity. This observation is in line with the idea of male-female differences in the susceptibility to chronic stress. Following CUMS exposure, mGR depleted mice exhibited a higher sensitivity to stress, displayed at the neuronal circuit level by a decrease in hippocampal PPR and LTP. The mechanism underlying the absence of LTP modulation by Intellicage induced CUMS in females and the sensitization to stress of mGR depleted mice, however, requires further investigation. One possible explanation behind the CUMS-induced LTP and PPR alterations observed in mGR depleted mice could result from differences observed in microglial morphology and homeostatic functions, in genes related to inflammation, as well as in neuronal connectivity. Further studies examining a possible compensatory mechanism in the neurons or other cells, i.e., an increased expression of the receptor that would sensitize them to stress, are also warranted. Moreover, while we found minimal physiological and neurobiological effects of CUMS in the WT mice hippocampus, we still observed a behavioral response in both genotypes with a decrease in both saccharine preference and motivated behavior, which suggest the CUMS paradigm might induce a neurobiological response recruiting other brain regions such as the nucleus accumbens, which is

involved in the sucrose preference (Scheggi et al., 2018). Overall, the mechanisms underlying modifications in short-and long-term plasticity of mGR depleted mice need further investigations.

5 Conclusion

Overall, our results demonstrate that microglial GR signaling contributes to neurogenesis and hippocampal synaptic connectivity while maintaining microglia in a surveillant state under steady-state condition. Our results also suggest that the lack of microglial GCs-GR does not alter the behavioral response to CUMS exposure, yet the underlying plasticity mechanisms and microglial gene profile are modified. These neural changes may compensate the deletion of microglial GR, allowing for an overall behavioral response to stress that is similar to the controls. Thus, mGR depleted mice still have the behavioral capacity to adapt to environmental challenges. These results support other findings (Frank et al., 2019; Hellwig et al., 2016; Kreisel et al., 2014; Milior et al., 2016) indicating that microglia are key players regulating the central nervous system response to chronic stress. Further studies are warranted to better understand the mechanisms underlying the effects of microglial GCs-GR signaling deficiency and to determine whether similar or different results would be seen in males and in other brain regions involved in the stress response (McEwen et al., 2015). Long-term consequences of chronic stress would also need to be investigated in our animal model. This study therefore suggests a mechanistic basis that could be used to modulate microglial activity and could help alleviate symptoms or prevent more severe neuropsychiatric disorders caused by chronic stress in females.

Acknowledgements

We acknowledge that Université Laval stands on the traditional and unceded land of the Huron-Wendat peoples; and that the University of Victoria exists on the territory of the Lekwungen peoples and that the Songhees, Esquimalt and WSÁNEÆ peoples have relationships to this land. We thank Emmanuel Planel for the access to the epifluorescence microscope and Julie-Christine Lévesque at the Bioimaging Platform of CRCHU de Québec-Université Laval for technical assistance. We also thank the Centre for Advanced Materials and Related Technology for the access to the confocal microscope with Airyscan. K.P. was supported by a doctoral scholarship from Fonds de Recherche du Québec – Santé (FRQS), an excellence award from Fondation du CHU de Québec, as well as from Centre Thématique de Recherche en Neurosciences and from Fondation Famille-Choquette. K.B. was supported by excellence scholarships from Université Laval and Fondation du CHU de Québec. S.G. is supported by FIRC-AIRC fellowship for Italy 22329/2018 and by Pilot ARISLA NKINALS 2019. C.W.H. and J.C.S. were supported by postdoctoral fellowships from FRQS. This study was funded by a Natural Sciences and Engineering Research Council of Canada (NSERC) Discovery grant (RGPIN-2014-05308) awarded to M.E.T., by ERANET neuron 2017 MicroSynDep to M.E.T. and I.B., and by the Italian Ministry of Health, grant RF-2018-12367249 to I.B, by PRIN 2017, AIRC 2019 and Ministero della Salute RF2018 to C.L . M.E.T. is a Tier II Canada Research Chair in *Neurobiology of Aging and Cognition.*

References

Alboni, S., Poggini, S., Garofalo, S., Milior, G., El Hajj, H., Lecours, C., Girard, I., Gagnon, S., Boisjoly-Villeneuve, S., Brunello, N., Wolfer, D.P., Limatola, C., Tremblay, M.-È., Maggi, L., Branchi, I., 2016. Fluoxetine treatment affects the inflammatory response and microglial function according to the quality of the living environment. Brain, Behavior, and Immunity 58, 261–271. https://doi.org/10.1016/j.bbi.2016.07.155

Alboni, S., van Dijk, R.M., Poggini, S., Milior, G., Perrotta, M., Drenth, T., Brunello, N., Wolfer, D.P., Limatola, C., Amrein, I., Cirulli, F., Maggi, L., Branchi, I., 2017. Fluoxetine effects on molecular, cellular and behavioral endophenotypes of depression are driven by the living environment. Molecular Psychiatry 22, 552–561. https://doi.org/10.1038/mp.2015.142

Bachstetter, A.D., Morganti, J.M., Jernberg, J., Schlunk, A., Mitchell, S.H., Brewster, K.W., Hudson, C.E., Cole, M.J., Harrison, J.K., Bickford, P.C., Gemma, C., 2011. Fractalkine and CX3CR1 regulate hippocampal neurogenesis in adult and aged rats. Neurobiol Aging 32, 2030–2044. https://doi.org/10.1016/j.neurobiolaging.2009.11.022

Basilico, B., Pagani, F., Grimaldi, A., Cortese, B., Angelantonio, S.D., Weinhard, L., Gross, C., Limatola, C., Maggi, L., Ragozzino, D., 2019. Microglia shape presynaptic properties at developing glutamatergic synapses. Glia 67, 53–67. https://doi.org/10.1002/glia.23508

Bessa, J.M., Ferreira, D., Melo, I., Marques, F., Cerqueira, J.J., Palha, J.A., Almeida, O.F.X., Sousa, N., 2009. The mood-improving actions of antidepressants do not depend on neurogenesis but are associated with neuronal remodeling. Mol Psychiatry 14, 764–773, 739. https://doi.org/10.1038/mp.2008.119

Bordeleau, M., Lacabanne, C., Fernández de Cossío, L., Vernoux, N., Savage, J.C., González-Ibáñez, F., Tremblay, M.-È., 2020. Microglial and peripheral immune priming is partially sexually dimorphic in adolescent mouse offspring exposed to maternal high-fat diet. J Neuroinflammation 17, 264. https://doi.org/10.1186/s12974-020-01914-1

Branchi, I., Santarelli, S., Capoccia, S., Poggini, S., D'Andrea, I., Cirulli, F., Alleva, E., 2013. Antidepressant treatment outcome depends on the quality of the living environment: a pre-clinical investigation in mice. PLoS One 8, e62226. https://doi.org/10.1371/journal.pone.0062226

Cadepond, F., PhD, Ulmann, A., MD, PhD, Baulieu, E.-E., MD, PhD, 1997. RU486 (MIFEPRISTONE): Mechanisms of Action and Clinical Uses. Annual Review of Medicine 48, 129–156. https://doi.org/10.1146/annurev.med.48.1.129

Carrillo-de Sauvage, M.Á., Maatouk, L., Arnoux, I., Pasco, M., Sanz Diez, A., Delahaye, M., Herrero, M.T., Newman, T.A., Calvo, C.F., Audinat, E., Tronche, F., Vyas, S., 2013. Potent and multiple regulatory actions of microglial glucocorticoid receptors during CNS inflammation. Cell Death Differ. 20, 1546–1557. https://doi.org/10.1038/cdd.2013.108

Carvalho-Netto, E.F., Myers, B., Jones, K., Solomon, M.B., Herman, J.P., 2011. Sex differences in synaptic plasticity in stress-responsive brain regions following chronic variable stress. Physiology & Behavior, 2010 Neurobiology of Stress Workshop 104, 242–247. https://doi.org/10.1016/j.physbeh.2011.01.024

Castro-Sánchez, S., García-Yagüe, Á.J., Kügler, S., Lastres-Becker, I., 2019. CX3CR1-deficient microglia shows impaired signalling of the transcription factor NRF2: Implications in tauopathies. Redox Biology 22, 101118. https://doi.org/10.1016/j.redox.2019.101118

Cherry, J.D., Olschowka, J.A., O'Banion, M.K., 2014. Neuroinflammation and M2 microglia: the good, the bad, and the inflamed. J Neuroinflammation 11, 98. https://doi.org/10.1186/1742-2094-11-98

Davis, M.T., Holmes, S.E., Pietrzak, R.H., Esterlis, I., 2017. Neurobiology of Chronic Stress-Related Psychiatric Disorders: Evidence from Molecular Imaging Studies. Chronic Stress (Thousand Oaks) 1. https://doi.org/10.1177/2470547017710916

de Kloet, E.R., Joëls, M., Holsboer, F., 2005. Stress and the brain: from adaptation to disease. Nature Reviews Neuroscience 6, 463–475. https://doi.org/10.1038/nrn1683

de Kloet, E.R., Karst, H., Joëls, M., 2008. Corticosteroid hormones in the central stress response: quick-and-slow. Front Neuroendocrinol 29, 268–272. https://doi.org/10.1016/j.yfrne.2007.10.002

Deak, T., Quinn, M., Cidlowski, J.A., Victoria, N.C., Murphy, A.Z., Sheridan, J.F., 2015. Neuroimmune mechanisms of stress: sex differences, developmental plasticity, and implications for pharmacotherapy of stress-related disease. Stress 18, 367–380. https://doi.org/10.3109/10253890.2015.1053451

Dong, Y., Wang, X., Zhou, Y., Zheng, Q., Chen, Z., Zhang, H., Sun, Z., Xu, G., Hu, G., 2020. Hypothalamus-pituitary-adrenal axis imbalance and inflammation contribute to sex differences in separation- and restraint-induced depression. Horm Behav 122, 104741. https://doi.org/10.1016/j.yhbeh.2020.104741

Egeland, M., Zunszain, P.A., Pariante, C.M., 2015. Molecular mechanisms in the regulation of adult neurogenesis during stress. Nat Rev Neurosci 16, 189–200. https://doi.org/10.1038/nrn3855

Eid, R.S., Lieblich, S.E., Duarte-Guterman, P., Chaiton, J.A., Mah, A.G., Wong, S.J., Wen, Y., Galea, L.A.M., 2020. Selective activation of estrogen receptors α and β: Implications for depressive-like phenotypes in female mice exposed to chronic unpredictable stress. Hormones and Behavior 119, 104651. https://doi.org/10.1016/j.yhbeh.2019.104651

Esch, T., Stefano, G.B., Fricchione, G.L., Benson, H., 2002. The role of stress in neurodegenerative diseases and mental disorders. Neuro Endocrinol. Lett. 23, 199–208.

Escoter-Torres, L., Caratti, G., Mechtidou, A., Tuckermann, J., Uhlenhaut, N.H., Vettorazzi, S., 2019. Fighting the Fire: Mechanisms of Inflammatory Gene Regulation by the Glucocorticoid Receptor. Front Immunol 10, 1859. https://doi.org/10.3389/fimmu.2019.01859

Fanselow, M.S., Dong, H.-W., 2010. Are The Dorsal and Ventral Hippocampus functionally distinct structures? Neuron 65, 7. https://doi.org/10.1016/j.neuron.2009.11.031

Ferragud, A., Haro, A., Sylvain, A., Velázquez-Sánchez, C., Hernández-Rabaza, V., Canales, J.J., 2010. Enhanced habit-based learning and decreased neurogenesis in the adult hippocampus in a murine model of chronic social stress. Behav. Brain Res. 210, 134–139. https://doi.org/10.1016/j.bbr.2010.02.013

Figueiredo, H.F., Dolgas, C.M., Herman, J.P., 2002. Stress Activation of Cortex and Hippocampus Is Modulated by Sex and Stage of Estrus. Endocrinology 143, 2534–2540. https://doi.org/10.1210/endo.143.7.8888

Filipello, F., Morini, R., Corradini, I., Zerbi, V., Canzi, A., Michalski, B., Erreni, M., Markicevic, M., Starvaggi-Cucuzza, C., Otero, K., Piccio, L., Cignarella, F., Perrucci, F., Tamborini, M., Genua, M., Rajendran, L., Menna, E., Vetrano, S., Fahnestock, M., Paolicelli, R.C., Matteoli, M., 2018. The Microglial Innate Immune Receptor TREM2 Is Required for

Synapse Elimination and Normal Brain Connectivity. Immunity 48, 979-991.e8. https://doi.org/10.1016/j.immuni.2018.04.016

Fourgeaud, L., Través, P.G., Tufail, Y., Leal-Bailey, H., Lew, E.D., Burrola, P.G., Callaway, P., Zagórska, A., Rothlin, C.V., Nimmerjahn, A., Lemke, G., 2016. TAM receptors regulate multiple features of microglial physiology. Nature 532, 240–244. https://doi.org/10.1038/nature17630

Frank, M.G., Fonken, L.K., Watkins, L.R., Maier, S.F., 2019. Microglia: Neuroimmune-sensors of stress. Seminars in Cell & Developmental Biology, SI: Calcium signalling 94, 176–185. https://doi.org/10.1016/j.semcdb.2019.01.001

Franklin, T.C., Wohleb, E.S., Zhang, Y., Fogaça, M., Hare, B., Duman, R.S., 2018. Persistent Increase in Microglial RAGE Contributes to Chronic Stress–Induced Priming of Depressive-like Behavior. Biological Psychiatry 83, 50–60. https://doi.org/10.1016/j.biopsych.2017.06.034

Füger, P., Hefendehl, J.K., Veeraraghavalu, K., Wendeln, A.-C., Schlosser, C., Obermüller, U., Wegenast-Braun, B.M., Neher, J.J., Martus, P., Kohsaka, S., Thunemann, M., Feil, R., Sisodia, S.S., Skodras, A., Jucker, M., 2017. Microglia turnover with aging and in an Alzheimer's model via long-term in vivo single-cell imaging. Nat. Neurosci. 20, 1371–1376. https://doi.org/10.1038/nn.4631

Galea, L.A., McEwen, B.S., Tanapat, P., Deak, T., Spencer, R.L., Dhabhar, F.S., 1997. Sex differences in dendritic atrophy of CA3 pyramidal neurons in response to chronic restraint stress. Neuroscience 81, 689–697. https://doi.org/10.1016/s0306-4522(97)00233-9

Garofalo, S., Porzia, A., Mainiero, F., Di Angelantonio, S., Cortese, B., Basilico, B., Pagani, F., Cignitti, G., Chece, G., Maggio, R., Tremblay, M.-E., Savage, J., Bisht, K., Esposito, V., Bernardini, G., Seyfried, T., Mieczkowski, J., Stepniak, K., Kaminska, B., Santoni, A., Limatola, C., 2017. Environmental stimuli shape microglial plasticity in glioma. Elife 6. https://doi.org/10.7554/eLife.33415

Garrett, J.E., Wellman, C.L., 2009. Chronic Stress Effects on Dendritic Morphology in Medial Prefrontal Cortex: Sex Differences and Estrogen Dependence. Neuroscience 162, 195–207. https://doi.org/10.1016/j.neuroscience.2009.04.057

Gemma, C., Bachstetter, A.D., 2013. The role of microglia in adult hippocampal neurogenesis. Front Cell Neurosci 7, 229. https://doi.org/10.3389/fncel.2013.00229

Golden, S.A., Covington, H.E., Berton, O., Russo, S.J., 2011. A standardized protocol for repeated social defeat stress in mice. Nat Protoc 6, 1183–1191. https://doi.org/10.1038/nprot.2011.361

Goldmann, T., Wieghofer, P., Müller, P.F., Wolf, Y., Varol, D., Yona, S., Brendecke, S.M., Kierdorf, K., Staszewski, O., Datta, M., Luedde, T., Heikenwalder, M., Jung, S., Prinz, M., 2013. A new type of microglia gene targeting shows TAK1 to be pivotal in CNS autoimmune inflammation. Nature Neuroscience 16, 1618–1626. https://doi.org/10.1038/nn.3531

Goshen, I., Kreisel, T., Ben-Menachem-Zidon, O., Licht, T., Weidenfeld, J., Ben-Hur, T., Yirmiya, R., 2008. Brain interleukin-1 mediates chronic stress-induced depression in mice via adrenocortical activation and hippocampal neurogenesis suppression. Molecular Psychiatry 13, 717–728. https://doi.org/10.1038/sj.mp.4002055

Gould, E., Tanapat, P., McEwen, B., Flügge, G., Fuchs, E., 1998. Proliferation of granule cell precursors in the dentate gyrus of adult monkeys is diminished by stress. Proceedings of

the National Academy of Sciences of the United States of America. https://doi.org/10.1073/PNAS.95.6.3168

Heck, A.L., Handa, R.J., 2019. Sex differences in the hypothalamic–pituitary–adrenal axis' response to stress: an important role for gonadal hormones. Neuropsychopharmacology 44, 45–58. https://doi.org/10.1038/s41386-018-0167-9

Hellwig, S., Brioschi, S., Dieni, S., Frings, L., Masuch, A., Blank, T., Biber, K., 2016. Altered microglia morphology and higher resilience to stress-induced depression-like behavior in CX3CR1-deficient mice. Brain, Behavior, and Immunity 55, 126–137. https://doi.org/10.1016/j.bbi.2015.11.008

Herman, J.P., McKlveen, J.M., Ghosal, S., Kopp, B., Wulsin, A., Makinson, R., Scheimann, J., Myers, B., 2016. Regulation of the hypothalamic-pituitary-adrenocortical stress response. Compr Physiol 6, 603–621. https://doi.org/10.1002/cphy.c150015

Hinwood, M., Morandini, J., Day, T.A., Walker, F.R., 2012. Evidence that microglia mediate the neurobiological effects of chronic psychological stress on the medial prefrontal cortex. Cereb. Cortex 22, 1442–1454. https://doi.org/10.1093/cercor/bhr229

Hinwood, M., Tynan, R.J., Charnley, J.L., Beynon, S.B., Day, T.A., Walker, F.R., 2013. Chronic stress induced remodeling of the prefrontal cortex: structural re-organization of microglia and the inhibitory effect of minocycline. Cereb. Cortex 23, 1784–1797. https://doi.org/10.1093/cercor/bhs151

Horchar, M.J., Wohleb, E.S., 2019. Glucocorticoid receptor antagonism prevents microglia-mediated neuronal remodeling and behavioral despair following chronic unpredictable stress. Brain Behav. Immun. 81, 329–340. https://doi.org/10.1016/j.bbi.2019.06.030

Hoshiko, M., Arnoux, I., Avignone, E., Yamamoto, N., Audinat, E., 2012. Deficiency of the Microglial Receptor CX3CR1 Impairs Postnatal Functional Development of Thalamocortical Synapses in the Barrel Cortex. J Neurosci 32, 15106–15111. https://doi.org/10.1523/JNEUROSCI.1167-12.2012

Hui, C.W., St-Pierre, M.-K., Detuncq, J., Aumailley, L., Dubois, M.-J., Couture, V., Skuk, D., Marette, A., Tremblay, J.P., Lebel, M., Tremblay, M.-È., 2018. Nonfunctional mutant Wrn protein leads to neurological deficits, neuronal stress, microglial alteration, and immune imbalance in a mouse model of Werner syndrome. Brain Behav. Immun. 73, 450–469. https://doi.org/10.1016/j.bbi.2018.06.007

Ibanez González, F., Picard, K., Bordelau, M., Sharma, K., Bisht, K., Tremblay, M.-È., 2019. Immunofluorescence Staining Using IBA1 and TMEM119 for Microglial Density, Morphology and Peripheral Myeloid Cell Infiltration Analysis in Mouse Brain. JoVE (Journal of Visualized Experiments) e60510. https://doi.org/10.3791/60510

Joëls, M., Krugers, H.J., 2007. LTP after stress: up or down? Neural Plast. 2007, 93202. https://doi.org/10.1155/2007/93202

Jp, A., Md, M., Mm, P.-B., 2000. Sexual dimorphism in the subiculum of the rat hippocampal formation. Brain Res 875, 125–137. https://doi.org/10.1016/s0006-8993(00)02605-6

Kim, J.J., Diamond, D.M., 2002. The stressed hippocampus, synaptic plasticity and lost memories. Nat. Rev. Neurosci. 3, 453–462. https://doi.org/10.1038/nrn849

Kiryk, A., Janusz, A., Zglinicki, B., Turkes, E., Knapska, E., Konopka, W., Lipp, H.-P., Kaczmarek, L., 2020. IntelliCage as a tool for measuring mouse behavior – 20 years perspective. Behavioural Brain Research 388, 112620. https://doi.org/10.1016/j.bbr.2020.112620

Kreisel, T., Frank, M.G., Licht, T., Reshef, R., Ben-Menachem-Zidon, O., Baratta, M.V., Maier, S.F., Yirmiya, R., 2014. Dynamic microglial alterations underlie stress-induced depressive-like behavior and suppressed neurogenesis. Molecular Psychiatry 19, 699–709. https://doi.org/10.1038/mp.2013.155

Lawson, L.J., Perry, V.H., Gordon, S., 1992. Turnover of resident microglia in the normal adult mouse brain. Neuroscience 48, 405–415. https://doi.org/10.1016/0306-4522(92)90500-2

Lecours, C., St-Pierre, M.-K., Picard, K., Bordeleau, M., Bourque, M., Awogbindin, I.O., Benadjal, A., Ibanez, F.G., Gagnon, D., Cantin, L., Parent, M., Di Paolo, T., Tremblay, M.-E., 2020. Levodopa partially rescues microglial numerical, morphological, and phagolysosomal alterations in a monkey model of Parkinson's disease. Brain Behav Immun 90, 81–96. https://doi.org/10.1016/j.bbi.2020.07.044

Lee, T., Jarome, T., Li, S.-J., Kim, J.J., Helmstetter, F.J., 2009. Chronic stress selectively reduces hippocampal volume in rats: a longitudinal MRI study. Neuroreport 20, 1554–1558. https://doi.org/10.1097/WNR.0b013e328332bb09

Lehmann, M.L., Cooper, H.A., Maric, D., Herkenham, M., 2016. Social defeat induces depressive-like states and microglial activation without involvement of peripheral macrophages. J Neuroinflammation 13. https://doi.org/10.1186/s12974-016-0672-x

Lightman, S.L., Conway-Campbell, B.L., 2010. The crucial role of pulsatile activity of the HPA axis for continuous dynamic equilibration. Nat Rev Neurosci 11, 710–718. https://doi.org/10.1038/nrn2914

Lin, Y., Westenbroek, C., Bakker, P., Termeer, J., Liu, A., Li, X., Ter Horst, G.J., 2008. Effects of long-term stress and recovery on the prefrontal cortex and dentate gyrus in male and female rats. Cereb Cortex 18, 2762–2774. https://doi.org/10.1093/cercor/bhn035

Liu, X., Quan, N., 2018. Microglia and CNS Interleukin-1: Beyond Immunological Concepts. Front Neurol 9, 8. https://doi.org/10.3389/fneur.2018.00008

Lotan, A., Lifschytz, T., Wolf, G., Keller, S., Ben-Ari, H., Tatarsky, P., Pillar, N., Oved, K., Sharabany, J., Merzel, T.K., Matsumoto, T., Yamawaki, Y., Mernick, B., Avidan, E., Yamawaki, S., Weller, A., Shomron, N., Lerer, B., 2018. Differential effects of chronic stress in young-adult and old female mice: cognitive-behavioral manifestations and neurobiological correlates. Molecular Psychiatry 23, 1432–1445. https://doi.org/10.1038/mp.2017.237

Maggi, L., Scianni, M., Branchi, I., D'Andrea, I., Lauro, C., Limatola, C., 2011. CX(3)CR1 deficiency alters hippocampal-dependent plasticity phenomena blunting the effects of enriched environment. Front Cell Neurosci 5, 22. https://doi.org/10.3389/fncel.2011.00022

Mazaheri, F., Snaidero, N., Kleinberger, G., Madore, C., Daria, A., Werner, G., Krasemann, S., Capell, A., Trümbach, D., Wurst, W., Brunner, B., Bultmann, S., Tahirovic, S., Kerschensteiner, M., Misgeld, T., Butovsky, O., Haass, C., 2017. TREM2 deficiency impairs chemotaxis and microglial responses to neuronal injury. EMBO Rep 18, 1186–1198. https://doi.org/10.15252/embr.201743922

McEwen, B.S., 2008. Central effects of stress hormones in health and disease: understanding the protective and damaging effects of stress and stress mediators. Eur J Pharmacol 583, 174–185. https://doi.org/10.1016/j.ejphar.2007.11.071

McEwen, B.S., 2001. Plasticity of the Hippocampus: Adaptation to Chronic Stress and Allostatic Load. Annals of the New York Academy of Sciences 933, 265–277. https://doi.org/10.1111/j.1749-6632.2001.tb05830.x

McEwen, B.S., Bowles, N.P., Gray, J.D., Hill, M.N., Hunter, R.G., Karatsoreos, I.N., Nasca, C., 2015. Mechanisms of stress in the brain. Nature Neuroscience 18, 1353–1363. https://doi.org/10.1038/nn.4086

McEwen, B.S., Gianaros, P.J., 2010. Central role of the brain in stress and adaptation: links to socioeconomic status, health, and disease. Ann N Y Acad Sci 1186, 190–222. https://doi.org/10.1111/j.1749-6632.2009.05331.x

McLaughlin, K.J., Baran, S.E., Wright, R.L., Conrad, C.D., 2005. Chronic stress enhances spatial memory in ovariectomized female rats despite CA3 dendritic retraction: Possible involvement of CA1 neurons. Neuroscience 135, 1045–1054. https://doi.org/10.1016/j.neuroscience.2005.06.083

Milior, G., Lecours, C., Samson, L., Bisht, K., Poggini, S., Pagani, F., Deflorio, C., Lauro, C., Alboni, S., Limatola, C., Branchi, I., Tremblay, M.-E., Maggi, L., 2016. Fractalkine receptor deficiency impairs microglial and neuronal responsiveness to chronic stress. Brain, Behavior, and Immunity, Microglia, Physiology and Behavior 55, 114–125. https://doi.org/10.1016/j.bbi.2015.07.024

Mitra, R., Sundlass, K., Parker, K.J., Schatzberg, A.F., Lyons, D.M., 2006. Social stress-related behavior affects hippocampal cell proliferation in mice. Physiology & Behavior 89, 123–127. https://doi.org/10.1016/j.physbeh.2006.05.047

Monfort, P., Gomez-Gimenez, B., Llansola, M., Felipo, V., 2015. Gender differences in spatial learning, synaptic activity, and long-term potentiation in the hippocampus in rats: molecular mechanisms. ACS Chem Neurosci 6, 1420–1427. https://doi.org/10.1021/acschemneuro.5b00096

Morais, M., Santos, P.A.R., Mateus-Pinheiro, A., Patrício, P., Pinto, L., Sousa, N., Pedroso, P., Almeida, S., Filipe, A., Bessa, J.M., 2014. The effects of chronic stress on hippocampal adult neurogenesis and dendritic plasticity are reversed by selective MAO-A inhibition. J Psychopharmacol 28, 1178–1183. https://doi.org/10.1177/0269881114553646

Munhoz, C.D., García-Bueno, B., Madrigal, J.L.M., Lepsch, L.B., Scavone, C., Leza, J.C., 2008. Stress-induced neuroinflammation: mechanisms and new pharmacological targets. Brazilian Journal of Medical and Biological Research 41, 1037–1046. https://doi.org/10.1590/S0100-879X2008001200001

Murray, F., Smith, D.W., Hutson, P.H., 2008. Chronic low dose corticosterone exposure decreased hippocampal cell proliferation, volume and induced anxiety and depression like behaviours in mice. European Journal of Pharmacology 583, 115–127. https://doi.org/10.1016/j.ejphar.2008.01.014

Olst, L. van, Bielefeld, P., Fitzsimons, C.P., Vries, H.E. de, Schouten, M., 2018. Glucocorticoid-mediated modulation of morphological changes associated with aging in microglia. Aging Cell 17, e12790. https://doi.org/10.1111/acel.12790

Orchinik, M., Murray, T.F., Moore, F.L., 1991. A corticosteroid receptor in neuronal membranes. Science 252, 1848–1851. https://doi.org/10.1126/science.2063198

Oyola, M.G., Handa, R.J., 2017. Hypothalamic-pituitary-adrenal and hypothalamic-pituitary-gonadal axes: sex differences in regulation of stress responsivity. Stress 20, 476–494. https://doi.org/10.1080/10253890.2017.1369523

Palumbo, M.C., Dominguez, S., Dong, H., 2020. Sex differences in hypothalamic–pituitary–adrenal axis regulation after chronic unpredictable stress. Brain and Behavior 10, e01586. https://doi.org/10.1002/brb3.1586

Patchev, V.K., Patchev, A.V., 2006. Experimental models of stress. Dialogues Clin Neurosci 8, 417–432.

Picard, K., St-Pierre, M.-K., Vecchiarelli, H.A., Bordeleau, M., Tremblay, M.-È., 2021. Neuroendocrine, neuroinflammatory and pathological outcomes of chronic stress: A story of microglial remodeling. Neurochem Int 145, 104987. https://doi.org/10.1016/j.neuint.2021.104987

Pisu, M.G., Garau, A., Boero, G., Biggio, F., Pibiri, V., Dore, R., Locci, V., Paci, E., Porcu, P., Serra, M., 2016. Sex differences in the outcome of juvenile social isolation on HPA axis function in rats. Neuroscience 320, 172–182. https://doi.org/10.1016/j.neuroscience.2016.02.009

Poggini, S., Golia, M.T., Alboni, S., Milior, G., Sciarria, L.P., Viglione, A., Matte Bon, G., Brunello, N., Puglisi-Allegra, S., Limatola, C., Maggi, L., Branchi, I., 2019. Combined Fluoxetine and Metformin Treatment Potentiates Antidepressant Efficacy Increasing IGF2 Expression in the Dorsal Hippocampus [WWW Document]. Neural Plasticity. https://doi.org/10.1155/2019/4651031

Reul, J.M., de Kloet, E.R., 1985. Two receptor systems for corticosterone in rat brain: microdistribution and differential occupation. Endocrinology 117, 2505–2511. https://doi.org/10.1210/endo-117-6-2505

Sapolsky, R.M., Krey, L.C., McEwen, B.S., 1985. Prolonged glucocorticoid exposure reduces hippocampal neuron number: implications for aging. J. Neurosci. 5, 1222–1227. https://doi.org/10.1523/JNEUROSCI.05-05-01222.1985

Scheggi, S., De Montis, M.G., Gambarana, C., 2018. Making Sense of Rodent Models of Anhedonia. Int J Neuropsychopharmacol 21, 1049–1065. https://doi.org/10.1093/ijnp/pyy083

Schloesser, R.J., Lehmann, M., Martinowich, K., Manji, H.K., Herkenham, M., 2010. Environmental enrichment requires adult neurogenesis to facilitate the recovery from psychosocial stress. Molecular Psychiatry 15, 1152–1163. https://doi.org/10.1038/mp.2010.34

Shimizu, S., Ishino, Y., Takeda, T., Tohyama, M., Miyata, S., 2019. Antidepressive Effects of Kamishoyosan through 5-HT1AReceptor and PKA-CREB-BDNF Signaling in the Hippocampus in Postmenopausal Depression-Model Mice. Evid Based Complement Alternat Med 2019, 9475384. https://doi.org/10.1155/2019/9475384

Sierra, A., Beccari, S., Diaz-Aparicio, I., Encinas, J.M., Comeau, S., Tremblay, M.-È., 2014. Surveillance, phagocytosis, and inflammation: how never-resting microglia influence adult hippocampal neurogenesis. Neural Plast 2014, 610343. https://doi.org/10.1155/2014/610343

Sierra, A., Encinas, J.M., Deudero, J.J.P., Chancey, J.H., Enikolopov, G., Overstreet-Wadiche, L.S., Tsirka, S.E., Maletic-Savatic, M., 2010. Microglia Shape Adult Hippocampal Neurogenesis through Apoptosis-Coupled Phagocytosis. Cell Stem Cell 7, 483–495. https://doi.org/10.1016/j.stem.2010.08.014

Sierra, A., Gottfried-Blackmore, A., Milner, T.A., McEwen, B.S., Bulloch, K., 2008. Steroid hormone receptor expression and function in microglia. Glia 56, 659–674. https://doi.org/10.1002/glia.20644

Singh, M.N., Martin-Hirsch, P.L., Martin, F.L., 2008. The multiple applications of tamoxifen: an example pointing to SERM modulation being the aspirin of the 21st century. Med. Sci. Monit. 14, RA144-148.

Smith, S.M., Vale, W.W., 2006. The role of the hypothalamic-pituitary-adrenal axis in neuroendocrine responses to stress. Dialogues in Clinical Neuroscience 8, 383.

Sorrells, S.F., Munhoz, C.D., Manley, N.C., Yen, S., Sapolsky, R.M., 2014. Glucocorticoids increase excitotoxic injury and inflammation in the hippocampus of adult male rats. Neuroendocrinology 100, 129–140. https://doi.org/10.1159/000367849

Sousa, R.J., Tannery, N.H., Lafer, E.M., 1989. In Situ Hybridization Mapping of Glucocorticoid Receptor Messenger Ribonucleic Acid in Rat Brain. Mol Endocrinol 3, 481–494. https://doi.org/10.1210/mend-3-3-481

Stellwagen, D., Beattie, E.C., Seo, J.Y., Malenka, R.C., 2005. Differential Regulation of AMPA Receptor and GABA Receptor Trafficking by Tumor Necrosis Factor-α. J Neurosci 25, 3219–3228. https://doi.org/10.1523/JNEUROSCI.4486-04.2005

Stellwagen, D., Malenka, R.C., 2006. Synaptic scaling mediated by glial TNF-α. Nature 440, 1054–1059. https://doi.org/10.1038/nature04671

Steptoe, A., Kivimäki, M., 2012. Stress and cardiovascular disease. Nature Reviews Cardiology 9, 360–370. https://doi.org/10.1038/nrcardio.2012.45

Tan, Y.-L., Yuan, Y., Tian, L., 2020. Microglial regional heterogeneity and its role in the brain. Molecular Psychiatry 25, 351–367. https://doi.org/10.1038/s41380-019-0609-8

Tanaka, J., Fujita, H., Matsuda, S., Toku, K., Sakanaka, M., Maeda, N., 1997. Glucocorticoid- and mineralocorticoid receptors in microglial cells: the two receptors mediate differential effects of corticosteroids. Glia 20, 23–37.

Tay, T.L., Savage, J.C., Hui, C.W., Bisht, K., Tremblay, M.-È., 2017. Microglia across the lifespan: from origin to function in brain development, plasticity and cognition. J. Physiol. (Lond.) 595, 1929–1945. https://doi.org/10.1113/JP272134

Tertil, M., Skupio, U., Barut, J., Dubovyk, V., Wawrzczak-Bargiela, A., Soltys, Z., Golda, S., Kudla, L., Wiktorowska, L., Szklarczyk, K., Korostynski, M., Przewlocki, R., Slezak, M., 2018. Glucocorticoid receptor signaling in astrocytes is required for aversive memory formation. Translational Psychiatry 8, 1–11. https://doi.org/10.1038/s41398-018-0300-x

Tremblay, M.-È., Lowery, R.L., Majewska, A.K., 2010. Microglial Interactions with Synapses Are Modulated by Visual Experience. PLoS Biology 8, e1000527. https://doi.org/10.1371/journal.pbio.1000527

Tremblay, M.-È., Zettel, M.L., Ison, J.R., Allen, P.D., Majewska, A.K., 2012. Effects of aging and sensory loss on glial cells in mouse visual and auditory cortices. Glia 60, 541–558. https://doi.org/10.1002/glia.22287

Vahrenkamp, J.M., Yang, C.-H., Rodriguez, A.C., Almomen, A., Berrett, K.C., Trujillo, A.N., Guillen, K.P., Welm, B.E., Jarboe, E.A., Janat-Amsbury, M.M., Gertz, J., 2018. Clinical and Genomic Crosstalk between Glucocorticoid Receptor and Estrogen Receptor α In Endometrial Cancer. Cell Rep 22, 2995–3005. https://doi.org/10.1016/j.celrep.2018.02.076

Vielkind, U., Walencewicz, A., Levine, J.M., Bohn, M.C., 1990. Type II glucocorticoid receptors are expressed in oligodendrocytes and astrocytes. J. Neurosci. Res. 27, 360–373. https://doi.org/10.1002/jnr.490270315

Weber, M.D., McKim, D.B., Niraula, A., Witcher, K.G., Yin, W., Sobol, C.G., Wang, Y., Sawicki, C.M., Sheridan, J.F., Godbout, J.P., 2019. The Influence of Microglial Elimination and Repopulation on Stress-Sensitization Induced by Repeated Social Defeat. Biol Psychiatry 85, 667–678. https://doi.org/10.1016/j.biopsych.2018.10.009

Wei, J., Yuen, E.Y., Liu, W., Li, X., Zhong, P., Karatsoreos, I.N., McEwen, B.S., Yan, Z., 2014. Estrogen protects against the detrimental effects of repeated stress on glutamatergic transmission and cognition. Molecular Psychiatry 19, 588–598. https://doi.org/10.1038/mp.2013.83

Wohleb, E.S., 2016. Neuron–Microglia Interactions in Mental Health Disorders: "For Better, and For Worse." Front. Immunol. 7. https://doi.org/10.3389/fimmu.2016.00544

Wohleb, E.S., Hanke, M.L., Corona, A.W., Powell, N.D., Stiner, L.M., Bailey, M.T., Nelson, R.J., Godbout, J.P., Sheridan, J.F., 2011. β-Adrenergic Receptor Antagonism Prevents Anxiety-Like Behavior and Microglial Reactivity Induced by Repeated Social Defeat. J. Neurosci. 31, 6277–6288. https://doi.org/10.1523/JNEUROSCI.0450-11.2011

Wohleb, E.S., McKim, D.B., Shea, D.T., Powell, N.D., Tarr, A.J., Sheridan, J.F., Godbout, J.P., 2014a. Re-establishment of Anxiety in Stress-Sensitized Mice Is Caused by Monocyte Trafficking from the Spleen to the Brain. Biol Psychiatry 75, 970–981. https://doi.org/10.1016/j.biopsych.2013.11.029

Wohleb, E.S., Patterson, J.M., Sharma, V., Quan, N., Godbout, J.P., Sheridan, J.F., 2014b. Knockdown of Interleukin-1 Receptor Type-1 on Endothelial Cells Attenuated Stress-Induced Neuroinflammation and Prevented Anxiety-Like Behavior. J Neurosci 34, 2583–2591. https://doi.org/10.1523/JNEUROSCI.3723-13.2014

Wohleb, E.S., Powell, N.D., Godbout, J.P., Sheridan, J.F., 2013. Stress-induced recruitment of bone marrow-derived monocytes to the brain promotes anxiety-like behavior. J. Neurosci. 33, 13820–13833. https://doi.org/10.1523/JNEUROSCI.1671-13.2013

Wohleb, E.S., Terwilliger, R., Duman, C.H., Duman, R.S., 2018. Stress-Induced Neuronal Colony Stimulating Factor 1 Provokes Microglia-Mediated Neuronal Remodeling and Depressive-like Behavior. Biological Psychiatry 83, 38–49. https://doi.org/10.1016/j.biopsych.2017.05.026

Woolley, C.S., Gould, E., McEwen, B.S., 1990. Exposure to excess glucocorticoids alters dendritic morphology of adult hippocampal pyramidal neurons. Brain Research 531, 225–231. https://doi.org/10.1016/0006-8993(90)90778-A

Yin, W., Gallagher, N.R., Sawicki, C.M., McKim, D.B., Godbout, J.P., Sheridan, J.F., 2019. Repeated social defeat in female mice induces anxiety-like behavior associated with enhanced myelopoiesis and increased monocyte accumulation in the brain. Brain Behav. Immun. 78, 131–142. https://doi.org/10.1016/j.bbi.2019.01.015

Zhou, X., Wahane, S., Friedl, M.-S., Kluge, M., Friedel, C.C., Avrampou, K., Zachariou, V., Guo, L., Zhang, B., He, X., Friedel, R.H., Zou, H., 2020. Microglia and macrophages promote corralling, wound compaction and recovery after spinal cord injury via Plexin-B2. Nature neuroscience 23, 337. https://doi.org/10.1038/s41593-020-0597-7

Zucker, R.S., 1989. Short-term synaptic plasticity. Annu. Rev. Neurosci. 12, 13–31. https://doi.org/10.1146/annurev.ne.12.030189.000305

Zuena, A.R., Mairesse, J., Casolini, P., Cinque, C., Alemà, G.S., Morley-Fletcher, S., Chiodi, V., Spagnoli, L.G., Gradini, R., Catalani, A., Nicoletti, F., Maccari, S., 2008. Prenatal restraint stress generates two distinct behavioral and neurochemical profiles in male and female rats. PLoS One 3, e2170. https://doi.org/10.1371/journal.pone.0002170

List of abbreviations

+: positive

-: negative

ABC: avidin-biotin complex

ACSF: artificial cerebrospinal fluid

AP-1: activator protein-1

AMPAR: AMPA receptor

ANOVA: analysis of variance

a.u.: arbitrary units

BDNF: brain-derived neurotrophic factor

BSA: bovine serum albumin

CA: *cornu ammonis*

CD: cluster of differentiation

CORT: corticosterone

Ct: cycle threshold

CUMS: chronic unpredictable mild stress

CX3CR1: CX3C chemokine receptor 1

DAB: 3,3’ diaminobenzidine

DCX: doublecortin

DG: dentate gyrus

EDTA: ethylenediaminetetraacetic acid

fEPSC: field excitatory postsynaptic currents

GAPDH: glyceraldehyde 3-phosphate dehydrogenase

GCs: glucocorticoids

GR: glucocorticoid receptor

HBSS: Hank's balanced salt solution

HFS: high-frequency stimulation

HPA: hypothalamic-pituitary-adrenal axis

IBA1: ionized calcium-binding adapter 1

IGF1: insulin-like growth factor

IL: interleukin

I/O: input/output

LPS: lipopolysaccharide

LTP: long-term potentiation

Mertk: myeloid-epithelial-reproductive tyrosine kinase

mGR : microglial-glucocorticoid receptor

mPFC: medial prefrontal cortex

MR: mineralocorticoid receptor

NF-κB: nuclear factor-κB

NMDAR: NMDA receptor

PBS: phosphate-buffered saline

PFA: paraformaldehyde

PPR: paired-pulse ratio

RT: room temperature

Rt-PCR: Real-time polymerase chain reaction

Str rad: *stratum radiatum*

SEM*:* standard error of the mean

TBS: Tris-buffered saline

TMEM119: Transmembrane Protein 119

Tnfα: and tumor necrosis factor α

Trem2: Triggering receptor expressed on myeloid cells

WT: wild-type

Figures, Tables and additional files

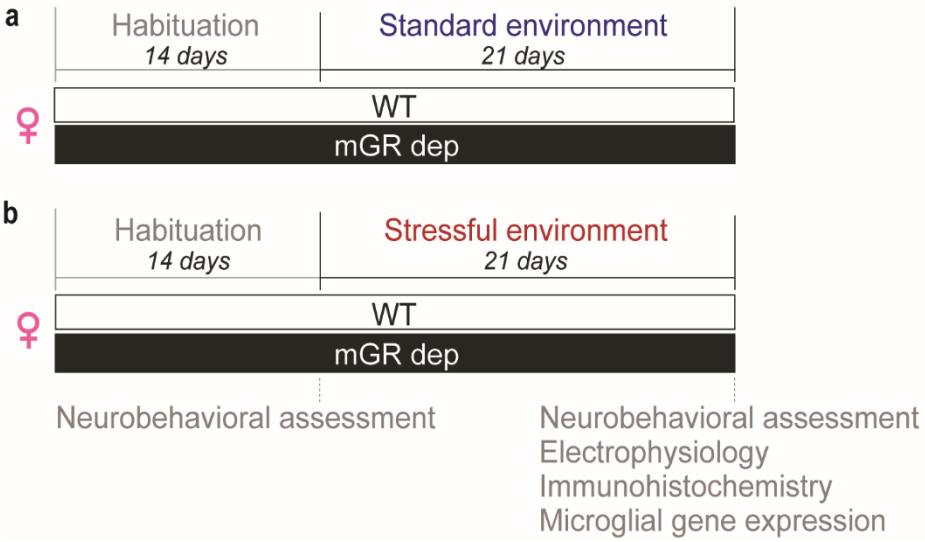

Figure 1. Schematic representation of the experimental design. Following 14-day period of habituation to the Intellicage system, the mice were exposed either to **(a)** standard or **(b)** stressful housing environment for 21-days. Immediately after the habituation phase and the environmental condition exposure, physiological and behavioral assessments were performed. At the end of the experiment, we performed a series of electrophysiological, immunohistological, and gene expression measures. mGR dep: microglial-glucocorticoid receptor depletion, WT: wild-type.

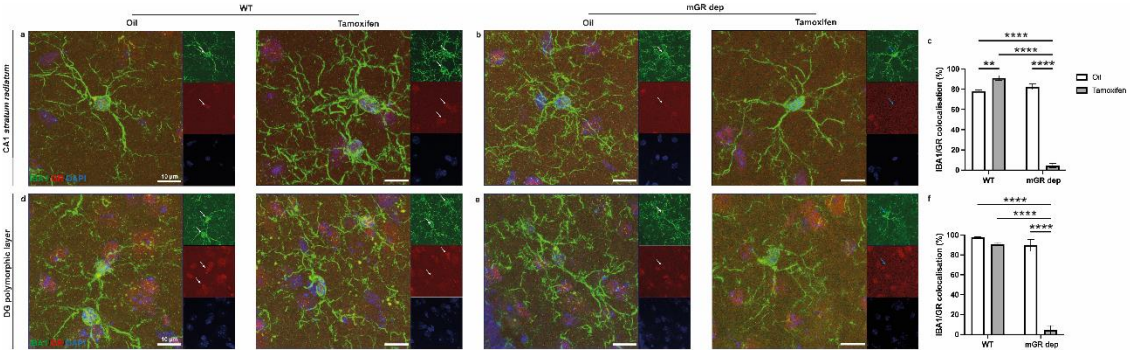

Figure 2. Characterization of microglial-GR depleted induced by tamoxifen. 4 weeks after the administration of tamoxifen or the vehicle, we used a double immunofluorescence with IBA1 and

GR to confirm microglial depletion of GR in the CA1 *str rad* (a, b, c) and DG polymorphic layer (d, e, f). The pictures were acquired using a confocal microscope (Zeiss LSM-880 with Airyscan) at a 63x magnification. Scale bar is equivalent to 10 µm. Data are shown as mean ± standard error of the mean (n=3-4 mice/group). White arrow: IBA1+/GR+ cell, blue arrow: IBA1+/GR- cell, DG: dentate gyrus, GR: glucocorticoid receptor, mGR dep: microglial-glucocorticoid receptor depletion, WT: wild-type. $^{**}p < 0.01$, $^{****}p < 0.0001$.

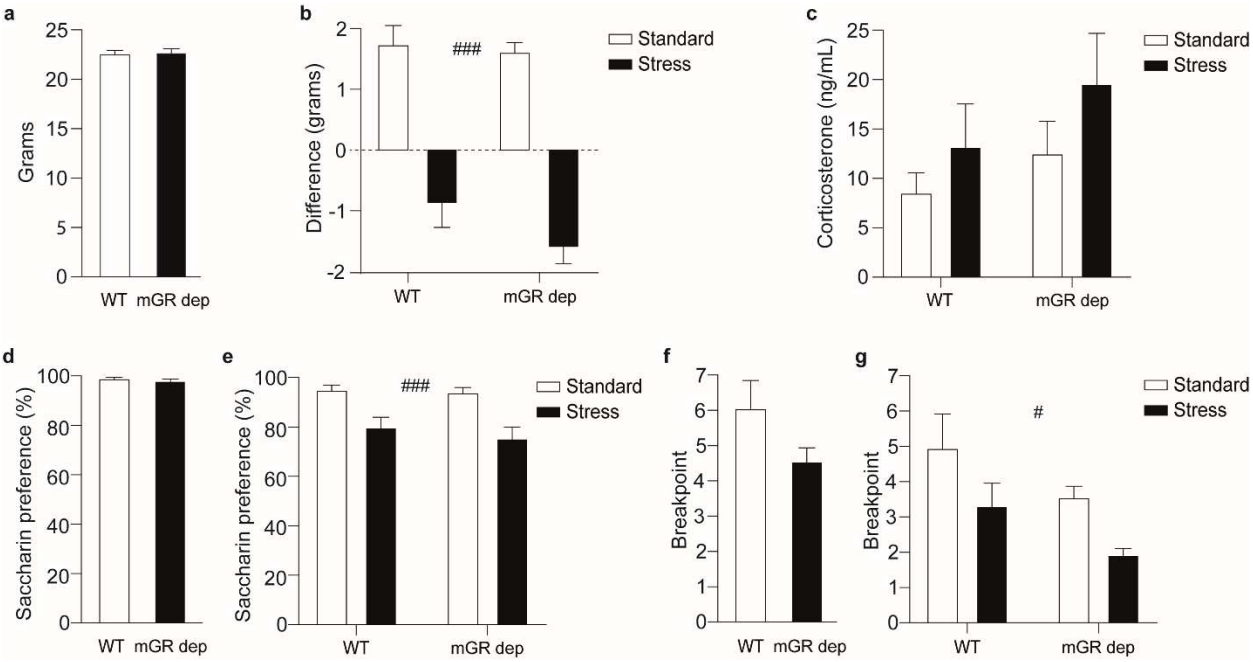

Figure 3. Physiological and behavioural responses of WT and microglial-GR depleted mice exposed to CUMS. (a) At the end of the habituation period, we did not observe difference of body weight between the groups. (b) Following the environment exposure, mGR dep and WT mice exposed to CUMS showed a significant reduction of body weight compared to the animals in standard condition. Inset represent environment effect. (c) The exposure to CUMS did not induced an increase in corticosterone levels. (d) During the habituation phase, both groups showed strong preference for the saccharin solution. (e) The exposure to the CUMS induced a significant decrease

of saccharine preference, with no difference between genotypes. (f) Before the exposure to the different environmental conditions, mGR depleted mice displayed a lower number of break point compared to the WT, but no significant difference was found. (g) At the end of the environmental condition, main effect of both genotype and condition was found. Data are shown as mean ± standard error of the mean (n=9-13 mice per group). CUMS: chronic unpredictable mild stress, mGR dep: microglial-glucocorticoid receptor depletion, WT: wild-type #p<0.05 and ### p<0.0001 *vs* standard.

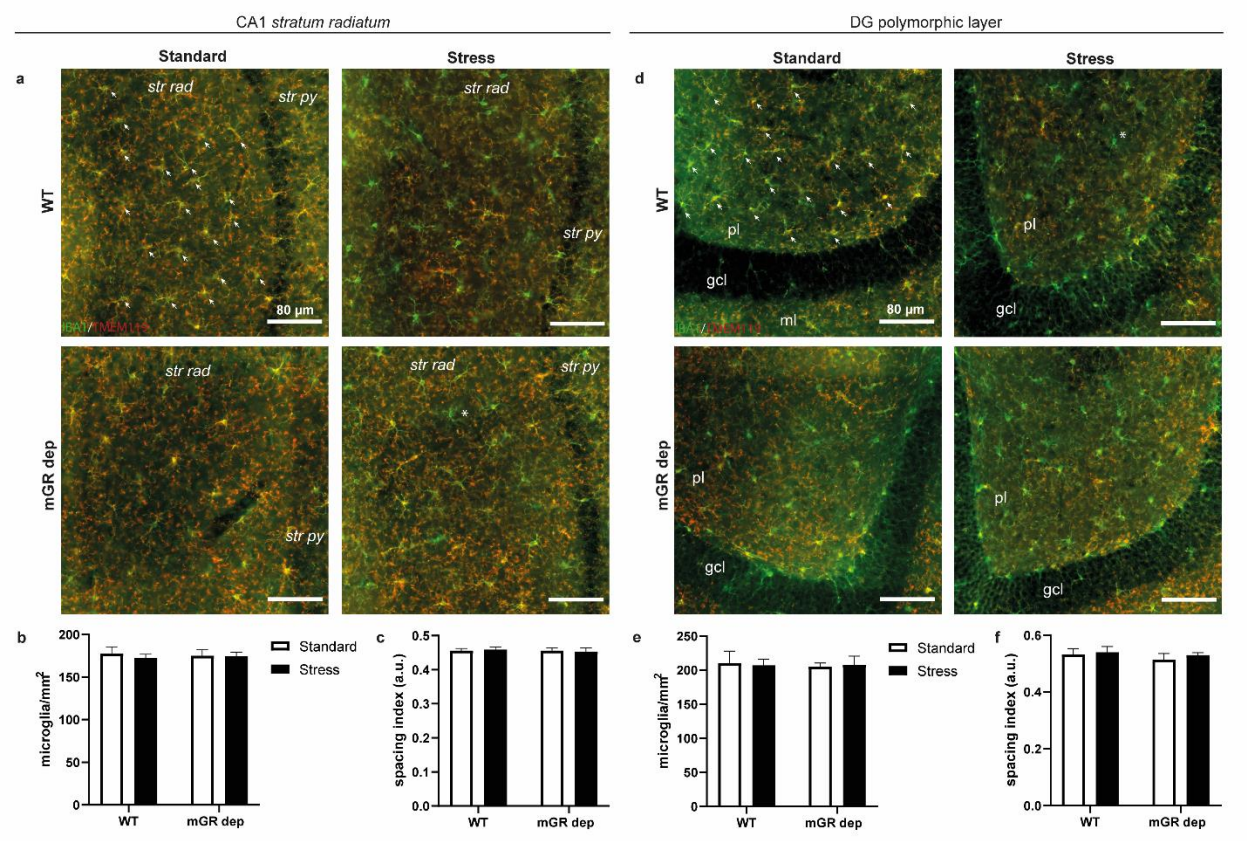

Figure 4. Density and distribution of microglia, perivascular, and infiltrating myeloid cells in WT *versus* microglial-GR depleted mice exposed to CUMS. Representative epifluorescence pictures at a 20x magnification showing IBA1- (green) and TMEM119- (red) stained microglia in CA1 *str rad* (a) and polymorphic layer of the dentate gyrus (d) in the four groups. Scale bar is

equivalent to 80 µm. White arrows: IBA1+/TMEM119- cells. No difference was observed for the microglial density and the spacing index in CA1 *str rad* (b,c) and in the polymorphic layer of the DG (e,f). (n=6 mice per group). Data are shown as mean ± standard error of the mean. a.u. = arbitrary units, CUMS: chronic unpredictable mild stress, DG: dentate gyrus, mGR dep: microglial-glucocorticoid receptor depletion, pl= polymorphic layer, gcl=granule cell layer, *str rad = stratum radiatum*, *str py = stratum pyramidale*, WT: wild-type.

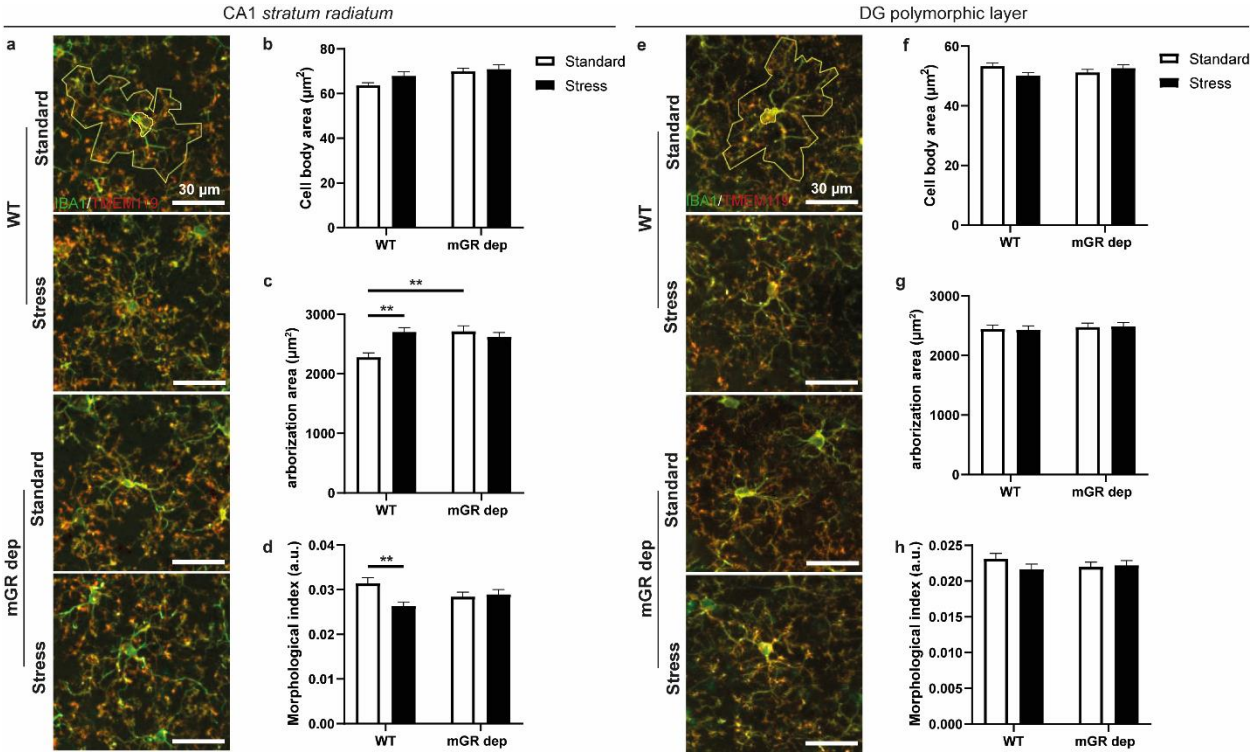

Figure 5. Microglial cell body and arborization area, as well as morphological index in WT *versus* microglial-GR depleted mice exposed to CUMS. Representative confocal pictures showing the morphology of IBA1- (green) and TMEM119- (red) stained microglia in the four groups, in the *CA1 str rad* (a) and the DG polymorphic layer (e) at a 20x magnification. Scale bar is equivalent to 30µm. Immunofluorescence of IBA1 (red) and TMEM119 (green) allowed the analysis of microglial cell body area (b,f), arborization area (c,g), and morphological index (d,h)

in the four groups, in both regions. Data are shown as mean ± standard error of the mean. (n=90-105 microglial cells in 6 mice per group). a.u. = arbitrary units, CUMS: chronic unpredictable mild stress, DG: dentate gyrus, mGR dep: microglial-glucocorticoid receptor depletion, *str rad* = *stratum radiatum*, WT: wild-type. $^{**}p < 0.01$.

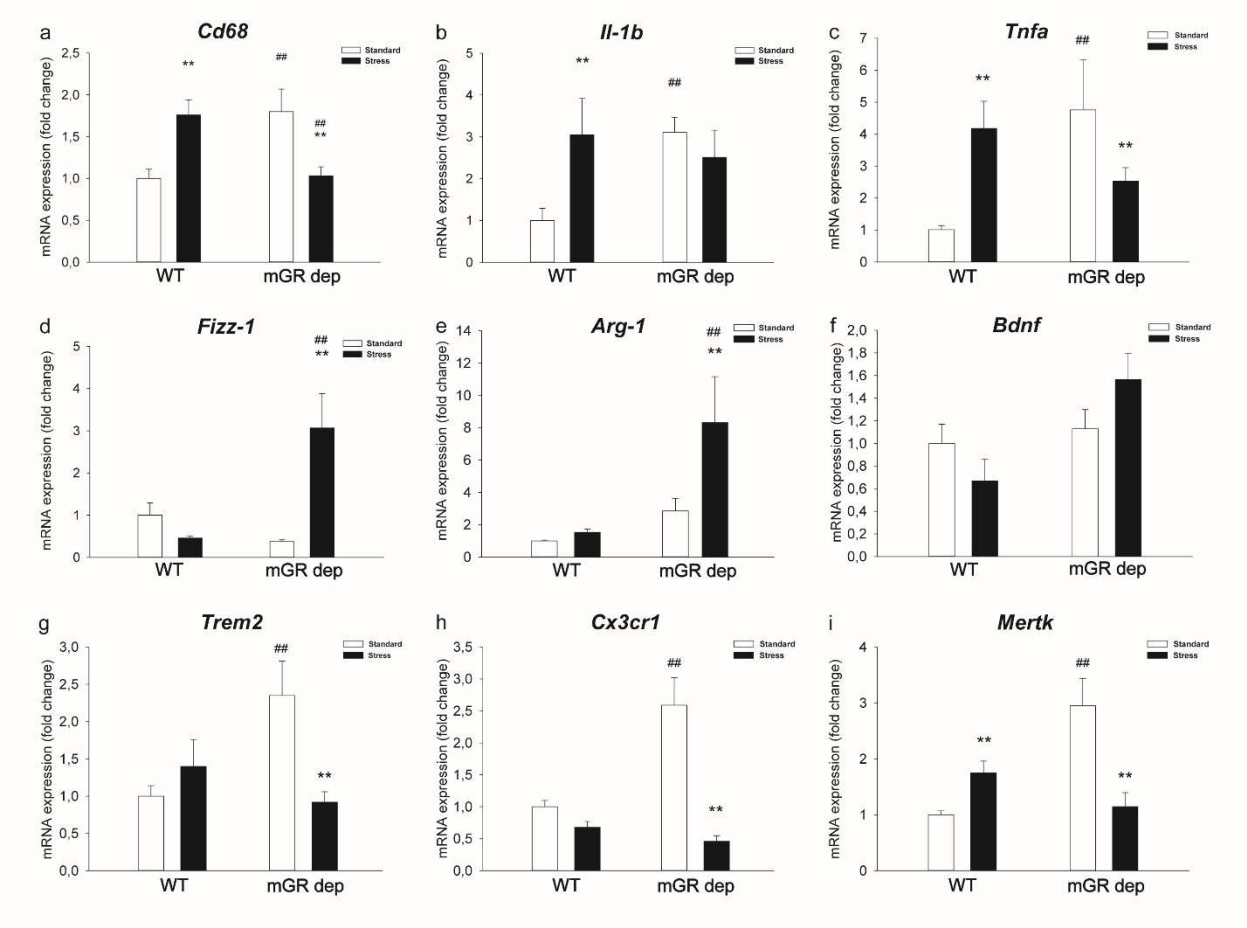

Figure 6. Gene expression changes in WT *versus* microglial-GR depleted mice exposed to CUMS. RT-PCR in CD11b^{+} cells sorted from hippocampus of WT or microglial-GR depleted mice of (a) *cd68*, (b) *il-1b*, (c) *tnfa*, (d) *fizz-1*, (e) *arg-1*, (f) *bdnf*, (g) *trem2*, (h) *cx3cr1* and (i) *mertk*. Data are shown as mean ± standard error of the mean (n=5 mice per group). Two-way ANOVA with Holm-sidak *post-hoc* test was used for the analysis. * Standard *vs* stress, # WT standard *vs* mGR depleted standard or WT stress *vs* mGR depleted stress. CUMS: chronic

unpredictable mild stress, mGR dep: microglial-glucocorticoid receptor depletion, Rt-PCR: Real-time polymerase chain reaction, WT: wild-type. *# $p<0.05$ **## $p<0.01$.

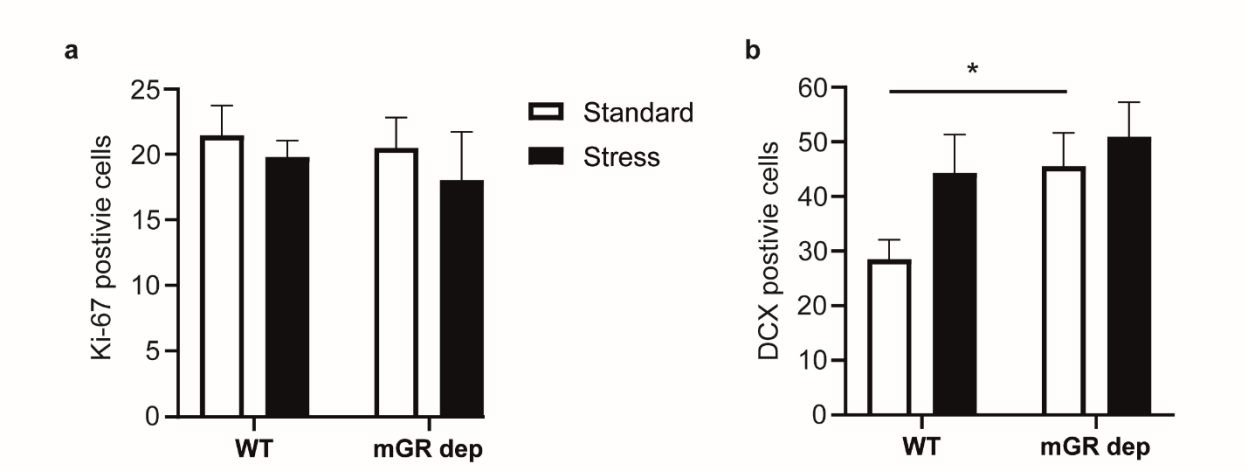

Figure 7. Adult neurogenesis levels in WT *versus* microglial-GR depleted mice exposed to CUMS. (a) Ki-67 and (b) DCX positive cells in the dentate gyrus. In the standard condition, DCX positive cells number is significantly lower in mGR depleted mice compared to WT. Data are shown as mean ± standard error of the mean (n=6 mice per group). CUMS: chronic unpredictable mild stress, DCX: doublecortin, mGR dep: microglial-glucocorticoid receptor depletion, WT: wild-type. *$p < 0.05$.

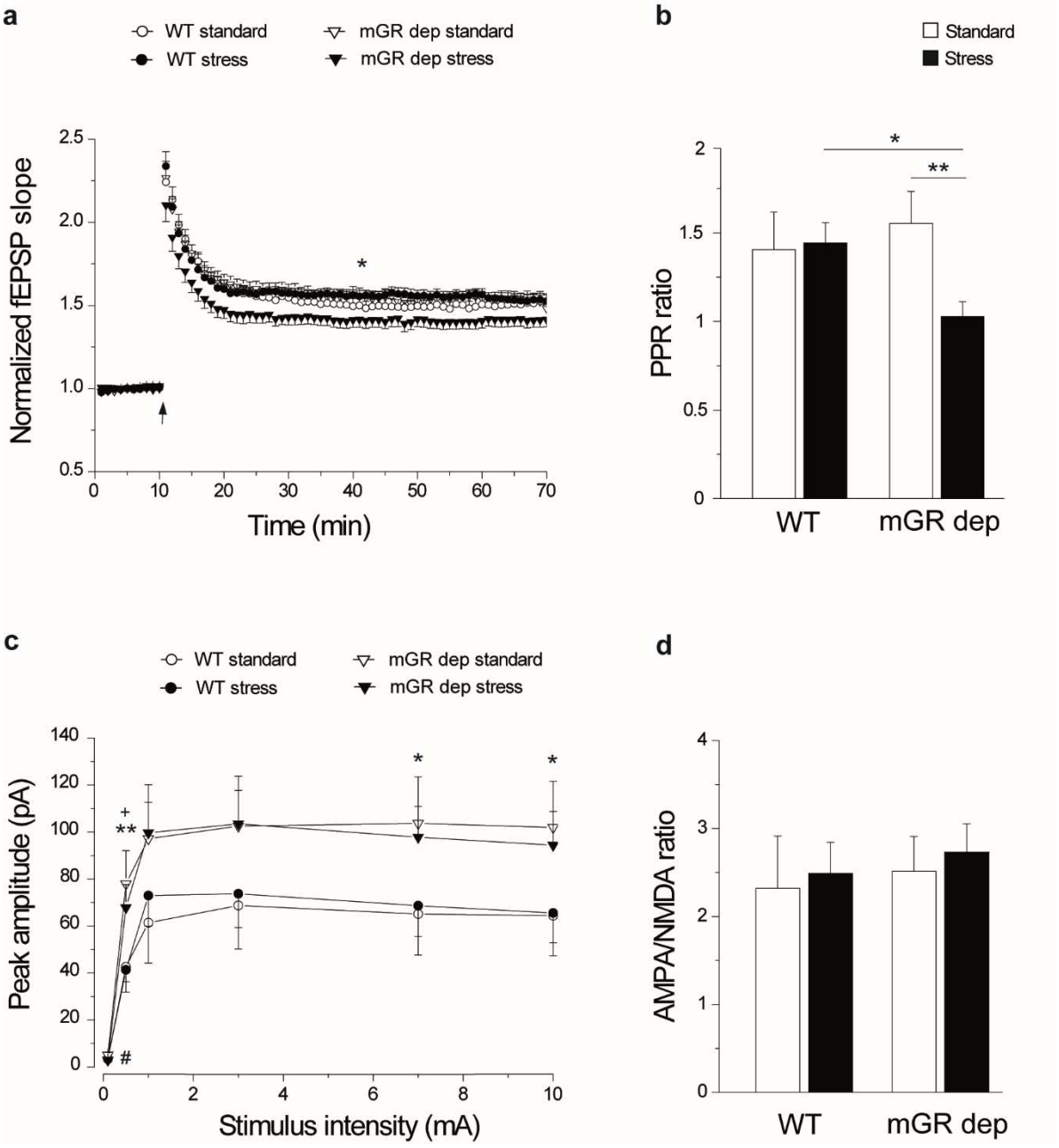

Figure 8. CA1 basal responses and synaptic plasticity in WT *versus* microglial-GR depleted mice exposed to CUMS. (a) LTP of fEPSP slope from extracellular records made from WT and mGR depleted mice exposed to standard or stress condition (WT standard n=16 slices/7 mice, white circle; WT stress n=14 slices/7 mice, black circles; mGR depleted standard n=14 slices/6 mice, white triangle; mGR depleted stress n=15 slices/6 mice, black triangle). Time course of slope

values from responses evoked at 0.05 Hz and normalized as detailed in the Methods. Arrows indicate LTP induction (HFS, 1 train of stimuli at 100 Hz, of 1 s duration). Data are means ± standard error of the mean. * $p<0.05$ mGR depleted stress *vs* mGR depleted standard or WT stress. (b) Histogram representing EPSC recorded in CA1 pyramidal cells in WT and mGR dep mice exposed to standard (white, n=13 slices/7 mice and n=14 slices/4 mice, respectively) and stressful (black, n=16 slices/5 mice and n=24 slices/6 mice, respectively) environment following paired-pulse stimulation of Schaffer collaterals (interstimulus interval 50 ms; average of 6 traces). Data are mean ± standard error of the mean. * $p<0.05$, ** $p<0.01$. (c) Relationship between stimulus intensity and evoked peak amplitudes of EPSC recorded at −70 mV from WT and mGR depleted mice exposed to standard and stress condition (WT standard n=13 slices/6 mice, white circle; WT stress n=16 slices/5 mice, black circles; mGR dep standard n=14 slices/4 mice, white triangle; mGR depleted stress n=23 slices/6 mice, black triangle). * $p<0.05$ ** p 0.01 WT *vs* mGR depleted, + $p<0.05$ WT standard *vs* mGR depleted standard, # $p<0.05$ mGR depleted standard *vs* mGR depleted stress. (d) Bar chart illustrating the ratio between AMPA current (evoked at −70 mV) and NMDA (evoked at +40 mV) in CA1 synapses, determined measuring EPSC amplitude in WT and mGR depleted following standard or stressful condition stimulation (WT standard n=8 slices/5 mice, WT stress n=13 slices/5 mice, mGR dep standard n=12 slices/4 mice and mGR depleted stress n=16 slices/6 mice). CUMS: chronic unpredictable mild stress, fEPSC: field excitatory postsynaptic currents, HFS: high-frequency stimulation, LTP: long-term potentiation, mA: milliampere, mGR dep: microglial-glucocorticoid receptor depletion, pA: peak amplitude, PPR: paired-pulse ratio, s: seconds, WT: wild-type.

Table 1. Primers sequence for real-time polymerase chain reaction experiments

Gene	***Primer Forward***	***Primer Reverse***
Arg1	CTCCAAGCCAAAGTCCTTAGAG	AGGAGCTGTCATTAGGGACATC
Cd68	AGAACTTACGGAAGCACCCA	GGCAGATATGCAGTCCCATT
Gapdh	TCGTCCCGTAGACAAAATGG	TTGAGGTCAATGAAGGGGTC
Il1b	GCAACTGTTCCTGAACTCAACT	ATCTTTTGGGGTCCGTCAACT
Tnfa	GTGGAACTGGCAGAAGAG	CCATAGAACTGATGAGAGG
Fizz-1	CAGGTCTGGCAATTCTTCTGAA	GTCTTGCTCATGTGTGTAAGTGA
Bdnf	CGGC GCCCATGAAAGAAGTA	AGACCTCTCGAA CCTGCCCT
Trem2	ATGGGACCTCTCCACCAGTT	TCACGTACCTCCGGGTCCA
Mertk	GATTCTGGCCAGCACAACAGA	GAGATATCCGGTAGCCCACCA
Cx3cr1	TGACTGGCACTTCCTGCAGA	AGGGCGTAGAAGACGGACAG

Table 2. Microglial distribution, perivascular and infiltrating myeloid cells and microglial process arborization properties in WT *versus* mGR depleted mice exposed to CUMS. % Infiltration: Average percentage of IBA1+/TMEM119- cells on total myeloid cells count, a.u.: arbitrary unit, CUMS: chronic unpredictable mild stress, DG: dentate gyrus, mGR dep: microglial-glucocorticoid receptor depletion, NND: nearest neighbor distance, *St rad*: *stratum radiatum*, WT: wild-type.

Parameters		Mean ± standard error of the mean				*F*	*p*
		Standard		Stress			
		WT	mGR dep	WT	mGR dep		
CA1 *St rad*	NND (a.u.)	50.846 ±0.898	51.339 ±0.899	51.896 ±0.858	51.246 ±0.523	Condition*Genotype: 0.4972 Condition: 0.3482 Genotype: 0.0093	Condition*Genotype: 0.4889 Condition: 0.5617 Gentoype: 0.9241
	% Infiltration	0.000 ±0.000	0.000 ±0.000	0.000 ±0.000	0.407 ±0.996	Condition*Genotype: 0.1667 Condition: 0.1667 Genotype: 0.1667	Condition*Genotype: 0.6874 Condition: 0.6874 Genotype: 0.6874
	Arborizations circularity (a.u.)	0.482 ±0.012	0.488 ±0.013	0.494 ±0.010	0.491 ±0.011	Condition*Genotype: 0.1448 Condition: 0.3911 Genotype: 0.0101	Condition*Genotype: 0.7038 Condition: 0.9199 Genotype: 0.5321
	Arborizations solidity (a.u.)	0.811 ±0.006	0.820 ±0.007	0.822 ±0.005	0.820 ±0.006	Condition*Genotype: 0.8006 Condition: 0.7718 Genotype: 0.2075	Condition*Genotype: 0.3715 Condition: .0.3802 Genotype: 0.6490
DG polymorphic layer	NND (a.u.)	51.015 ±1.764	50.488 ±1.120	51.516 ±0.896	51.535 ±1.691	Condition*Genotype: 0.0371 Condition: 0.2982	Condition*Genotype: 0.8491 Condition: 0.5911

						Genotype: 0.0320	Genotype: 0.8598
	% Infiltration	0.000 ±0.000	0.000 ±0.000	0.407 ±0.996	0.340 ±0.833	Condition*Genotype: 0.0026 Condition: 0.3307 Genotype: 0.0026	Condition*Genotype: 0.9597 Condition: 0.5716 Genotype: 0.9597
	Arborizations circularity (a.u.)	0.544 ±0.010	0.560 ±0.011	0.518 ±0.011	0.524 ±0.011	Condition*Genotype: 0.1908 Condition: 8.288 Genotype: 1.097	Condition*Genotype: 0.3325 Condition: **0.0042** Genotype: 0.2956
	Arborizations solidity (a.u.)	0.846 ±0.005	0.855 ±0.005	0.833 ±0.006	0.830 ±0.005	Condition*Genotype: 1.329 Condition: 13.460 Genotype: 0.3546	Condition*Genotype: 0.2498 Condition: **0.0003** Genotype: 0.5518

Supplementary material

Estrous cycle monitoring

Methods

Considering the potential effect of hormonal fluctuation on the behavioral outcomes, we evaluated the estrous cycle of the animals. Vaginal smear was collected by lavage of the vagina with a saline solution using a Gilson pipette, processed with methylene blue stain, and analyzed using light microscopy. The estrous cycle was consistently assessed at the same time, between 10:00 and 12:00 a.m., prior to the stress exposure as well as during the CUMS exposure at days 7 and 21.

Results

No association was found suggesting that the behavioral responses were not affected by the estrous phase (data not shown).

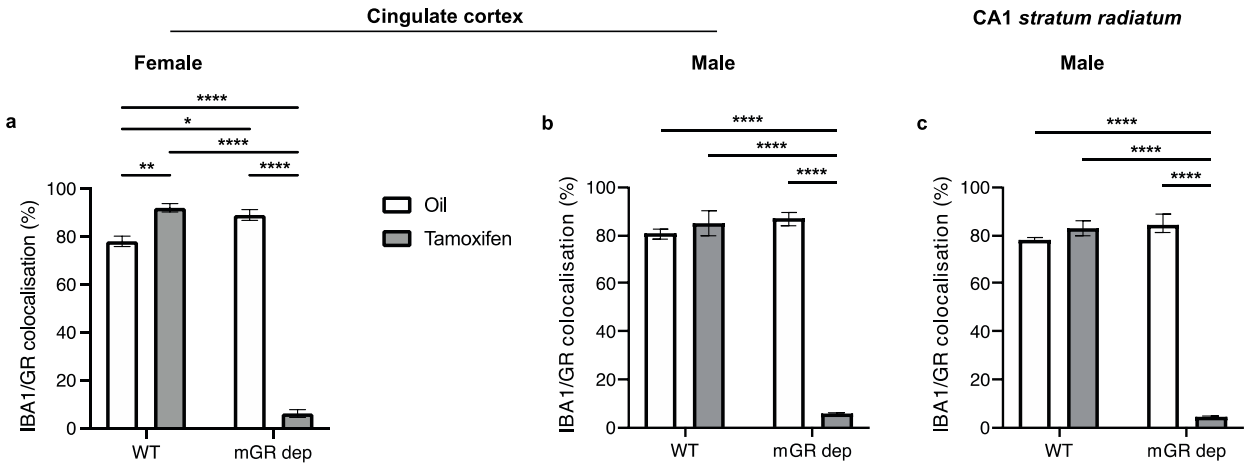

Supplementary Figure 1. Characterization of microglial GR depletion induced by tamoxifen

4 weeks after the administration of tamoxifen or vehicle, we used a double immunofluorescence with IBA1 and GR to confirm the depletion of microglial GR in the cingulate cortex in (a) female and male (b) mice, and in CA1 *str rad* (b) in male mice. Data are shown as mean ± standard error of the mean (n=3-5 mice/group). GR: glucocorticoid receptor, mGR dep: microglial-glucocorticoid receptor depletion, WT: wild-type. ****$p < 0.0001$.